Incorporating state-dependent Temperature–Salinity constraints in the background error covariance of variational ocean data assimilation

S. Ricci[1], A. T. Weaver[1], J. Vialard[2] and P. Rogel[1]

Research Department

[1] *Centre Européen de Recherche et de Formation Avancée en Calcul Scientifique (CERFACS/CNRS, URA 1875 - SUC), Toulouse, France.*
[2] *Laboratoire d'Océanographie Dynamique et de Climatologie (UMR CNRS/IRD/UPMC), Paris, France.*

Abstract

Several studies have illustrated how the univariate assimilation of temperature data can have a detrimental effect on the ocean state variables (salinity, currents) not directly constrained by the data. In this paper, we describe how the salinity adjustment method proposed by Troccoli and Haines (1999) can be included as a multivariate temperature-salinity (T–S) constraint within a background-error covariance model for variational data assimilation. The method is applied to a three-dimensional variational assimilation (3D-Var) system for a tropical Pacific version of the OPA ocean general circulation model. An identical twin experiment is presented first to illustrate how the method is effective in reconstructing a density profile using only temperature observations from that profile. The 3D-Var system is then cycled over the period 1993-98 using *in situ* temperature data from the Global Temperature and Salinity Pilot Programme. Relative to a univariate (T) 3D-Var, the multivariate (T, S) 3D-Var significantly improves the salinity mean state. A comparison with salinity data that are not assimilated is also presented. The fit to these observations is improved when the T–S constraint is applied. The salinity correction leads to a better preservation of the salinity structure and avoids the development of spurious geostrophic currents which were evident in the univariate analysis. The currents at the surface and below the core of the undercurrent are also improved.

Examination of the heat budget highlights how, in the univariate experiment, the temperature increment must compensate for a perpetual degradation of the temperature field by abnormally strong advection in the univariate experiment. When the T–S constraint is applied, this spurious advection is reduced and the mean temperature increment is decreased. Examination of the salt budget shows that spurious advection is also the main cause of the upper ocean freshening. When the T–S constraint is applied, the salinity structure is improved allowing for a better representation of the advection term and better preservation of the salt content in the upper ocean. The T–S constraint does not correct for all problems linked to data assimilation: vertical mixing is still too strong, and the surface salinity state and currents still have substantial errors. Improvements can be expected by including additional constraints in the background error covariances and by assimilating salinity data.

1 Introduction

In the tropics, salinity effects have often been neglected when studying the ocean general circulation. Looking at averaged conditions this assumption is justified: the change in density due to changes in temperature is much greater than the change in density due to changes in salinity. Nevertheless, several studies have shown that salinity can play an important role in the variability of the tropical oceans. For example, Roemmich *et al.* (1994) have shown that salinity induced zonal pressure gradients can contribute significantly to equatorial jets in the Pacific. Studies by Lukas and Lindström (1991) and Vialard and Delecluse (1998a, b) have illustrated that salinity can influence the heat and momentum budget of the upper ocean in the western Pacific through its effects on vertical stratification.

Any accurate description of the ocean state should then include salinity. In the context of data assimilation, Derber and Rosati (1989) and Troccoli and Haines (1999) noted that in regions of low vertical stability, correcting only the temperature field can make the density profile unstable, leading to an artificial enhancement of convection and vertical mixing, and the creation of spurious water masses. Troccoli *et al.* (2002) illustrate how this problem can severely degrade both temperature and salinity below the thermocline in the equatorial region when assimilating temperature data with a univariate optimal interpolation (OI) scheme. Ji *et al.* (2000) showed that assimilating sea-level anomaly (SLA) and temperature data by correcting temperature only with a univariate three-dimensional variational (3D-Var) scheme can improve sea level variability but at the expense of reducing the accuracy of the temperature field. They attributed this problem to the absence of a salinity correction in the analysis problem.

Degrading the salinity state can lead to significant errors in the velocity field as discussed by Cooper (1988). This has been illustrated by Vialard *et al.* (2003) using a univariate 3D-Var system similar to the one applied here. In that study it was shown that the univariate 3D-Var could produce a good analysis of temperature but at the expense of degrading many aspects of the salinity and velocity fields. In particular, the mean salinity state in the upper 300m displayed a significant drift of 0.2 psu over their 6-year analysis period and the equatorial currents a large eastward bias of 0.2ms^{-1} at the surface. These problems were attributed to a false circulation cell that was generated by data assimilation. The cause of this false cell will be further explored in this study.

Any effort to correct the salinity field through data assimilation must confront the scarcity of direct observations of salinity, although the situation is now changing with the deployment of Argo profiling floats (Roemmich *et al.* 2001). The main components of the ocean observing system are measurements of temperature from *in situ* and satellite platforms and of sea level from altimetry. One must then find a way to estimate the salinity when only temperature and/or sea level information are available. One approach for estimating salinity is to use a local climatological relation between temperature (T) and salinity (S) provided by observations. This approach is justified in certain areas of the global ocean where T–S water mass properties are conserved over long periods of time (Troccoli and Haines 1999). The disadvantage with this approach is that it does not allow for any variability in the T–S relation.

Vossepoel and Behringer (2000) propose a method to correct salinity through the assimilation of SLA using a 3D-Var scheme. SLA was related to salinity (and temperature) through dynamic height which was applied in the observation operator of the 3D-Var cost function. Information from SLA could then be transferred onto both temperature and salinity through the action of the adjoint of the observation operator in the 3D-Var analysis step. Without observations of SLA, however, their scheme is unable to correct salinity since the background-error covariances for temperature and salinity are taken to be mutually uncorrelated. The vertical structure of the salinity correction was determined by the background salinity error variance which was taken to be depth dependent and specified from statistics of the observed climatology of Conductivity-Temperature-Depth (CTD) profiles. Maes *et al.* (2000) and Maes and Behringer (2000) describe an alternative technique for estimating salinity using coupled T–S Empirical Orthogonal Functions (EOFs) derived from historical CTD data-sets. Since salinity observations are scarce and regionally confined, such an EOF analysis will generally not be relevant for all oceanic regions. Troccoli and Haines (1999) (hereafter referred to as TH99) propose a salinity adjustment method that uses the local T–S relation taken from the model background state to derive a salinity correction from an OI-computed temperature analysis. Their scheme was shown to be effective in reducing artificial vertical mixing and in maintaining the structure of the thermocline and halocline.

The present study aims at extending the salinity adjustment method of TH99 to the variational data assimilation system of Weaver *et al.* (2003). This method was favoured over the other methods presented above since it can be applied in a global system, allows for state (flow) dependency in the T–S relation, and does not require any prior statistical analysis of an observational data-base. In this study, we discuss how the T–S relation can be introduced as a multivariate constraint in the background-error covariance matrix, thereby allowing temperature and salinity to be corrected simultaneously in the variational analysis step. In this respect, our approach differs from that of TH99 where the T–S constraint was designed to compute a correction to salinity after the analysis of temperature.

The outline of the paper is as follows. Section 2 describes the assimilation system, paying particular attention to the general multivariate formulation of the background-error covariance matrix. Section 3 details the flow-dependent T–S constraint used in the covariance model, and illustrates its properties in a simple example using simulated data from a single temperature profile. 3D-Var experiments with and without the T–S constraint are presented in section 4 and the impact of the T–S constraint on the ocean mean state is assessed. In section 5 the heat and fresh water budgets are investigated to quantify how the extra heat and salt sources associated with the analysis increment act to change the dynamical balances in the model. A summary and discussion are given in section 6.

2 The assimilation system

2.1 Model and forcing

The ocean model used in this study is the rigid-lid version of the OPA OGCM of the Laboratoire d'Océanographie Dynamique et de Climatologie (LODYC; Madec *et al.* 1998). The model solves the primitive equations for horizontal currents $\mathbf{u}_h = (u, v)^T$, potential temperature T, and salinity S.[1] The equations are formulated in orthogonal curvilinear z-coordinates and discretised using finite differences on an Arakawa C-grid. The configuration of the model used here covers the tropical Pacific from 120°E to 70°W and 30°S to 30°N. The zonal resolution is 1° and the meridional resolution varies from 0.5° at the equator to 2° at artificial solid boundaries at 30°S and 30°N. The vertical resolution is divided into 25 levels, with grid depths ranging from 10m in the upper 130m to 1000m in the deep ocean. More details about this configuration of the model can be found in Vialard *et al.* (2001).

In the present study, the model is forced over the 6-year period from 1993-98 using wind-stress derived from a combined weekly ERS-TAO (European Remote Sensing satellite - Tropical Atmosphere-Ocean array) wind product (Vialard *et al.* 2002), daily fields of heat flux and evaporation from the National Centers for Environmental Prediction re-analysis (Kalnay *et al.* 1996), and monthly precipitations from the Global Precipitation Climatology Project (Huffman *et al.* 1997). The initial conditions on 1 January 1993 were obtained from a spin-up of the model as described in Vialard *et al.* (2002). They showed that a good simulation of the sea surface salinity (SSS) could be achieved with the above forcing combined with a flux correction strategy. Since we are also concerned with an accurate estimate of the salinity field in this study, we will follow the same approach. Each experiment in this paper is first run with a relaxation both to weekly sea surface temperature (SST) analyses from Reynolds and Smith (1994) and to monthly climatological SSS from Levitus *et al.* (1994). A relaxation coefficient of -40 W.m^{-2}.K^{-1} is used for SST, which corresponds to a restoring time-scale of one month for a depth scale of 50 m. The relaxation coefficient used for SSS was chosen to give an equivalent restoring time scale to that for SST. At the end of each experiment, the 1993-98 monthly climatology of the SSS relaxation term was computed and added as a flux correction to the fresh water surface forcing. The experiments were then repeated without relaxation to SSS (but still retaining relaxation to SST). This strategy avoids large drifts of the SSS, while leaving it free to vary at interannual timescales.

It should be noted that this set of surface forcing is different from the one used in Weaver *et al.* (2003) and Vialard *et al.* (2003). For this reason, results presented in those two papers can only be compared qualitatively with those presented here. The impact of the different forcing fields is addressed in section 4.2.

2.2 Assimilation and validation data-sets

The observations used for assimilation consist of *in situ* temperature measurements from the Global Temperature and Salinity Pilot Project (GTSPP) of the National Oceanographic Data Center, and are the same data used by Weaver *et al.* (2003) and Vialard *et al.* (2003). This data-set includes measurements mainly from TAO moorings and Expendable Bathy-Thermographs (XBTs), plus a limited number of CTD casts and drifting buoys. A manual quality control procedure was used to remove suspect data.

Salinity observations are not assimilated in this study but are used for validation. The Levitus *et al.* (1994) climatology (hereafter referred to simply as Levitus) is used as an observational reference. While this data-set does not allow for fine-scale validations of the analysed variability, it will allow us to diagnose gross errors

---

[1]Note that a *superscript T* will be used throughout the paper to indicate the transpose of a matrix or vector, whereas a *subscript T* or *variable T* will be used to refer to the model temperature field.

in the salinity analysis. Some additional observations are obtained from the Johnson *et al.* (2002) data-set compiled at the Pacific Marine Environment Laboratory. This data-set includes approximatively 3000 CTD profiles irregularly distributed over the 1993-98 period.

Current data from the TAO array will also be used for validation in this study. A description of these data and associated calibration procedures can be found in McPhaden *et al.* (1998). The comparison between the model results and the current data was performed by generating model averages using the same sampling as available for the current data.

2.3 Assimilation method

The assimilation method used in this study is an FGAT (First Guess at Appropriate Time) version of 3D-Var (Weaver *et al.* 2003). A description of the method is given below in order to highlight the specific extensions made to the method in the present study.

Let $\mathbf{x} = (\mathbf{u}_h^T, T, S)^T$ denote the ocean model state vector. In what follows, it is important to distinguish $\mathbf{x}$, which contains the 3D prognostic model variables, from the analysis vector $\mathbf{w}$, which contains only those components of $\mathbf{x}$ that are to be estimated from the observations using the assimilation method. (The notation used in this section closely follows the recommendations of Ide *et al.* (1997)).

In the 3D-Var of Weaver *et al.* (2003), the analysis was univariate, the only analysis variable being the 3D temperature field ($\mathbf{w} = T$). The analysis was univariate since the formulation of the background-error covariance matrix ($\mathbf{B}_{(\mathbf{w})}$) was univariate and since only temperature data were assimilated. In this study, we continue to assimilate only temperature data but now develop a multivariate formulation of $\mathbf{B}_{(\mathbf{w})}$ to include constraints between temperature and salinity. This is sufficient to generate a salinity analysis in 3D-Var in the absence of direct salinity observations (see section (2.4)). The analysis vector in this study is thus $\mathbf{w} = (T, S)^T$.

Let $\mathbf{w}^b = (T^b, S^b)^T$ denote the background estimate of $\mathbf{w}$ at analysis time. In 3D-Var, the objective is to determine the vector $\mathbf{w}$ that leads to the best simultaneous fit, in a statistically weighted least squares sense, to the observation vector $\mathbf{y}^o$ (here temperature) and to $\mathbf{w}^b$. While the 3D-Var analysis is static, the observations that are assimilated are usually distributed over a given time window $t_0 \leq t_i \leq t_n$; i.e., $\mathbf{y}^o = ((\mathbf{y}_0^o)^T, ..., (\mathbf{y}_i^o)^T, ..., (\mathbf{y}_n^o)^T)^T$ where $\mathbf{y}_i^o$ denotes the observation vector at time t_i. The fact that the measurement time of the observation may be different from the time of the background can be a source of bias in the 3D-Var analysis. The FGAT version of 3D-Var is an incremental algorithm designed to overcome this problem by allowing the observations to be compared with the background state at their appropriate time.

In 3D-Var FGAT, we seek to compute an increment $\delta \mathbf{w} = \mathbf{w} - \mathbf{w}^b$ that minimizes a quadratic cost function of the form $J = J_b + J_o$ where

$$J_b = \frac{1}{2} \delta \mathbf{w}^T \mathbf{B}_{(\mathbf{w})}^{-1} \delta \mathbf{w} \qquad \text{and} \qquad J_o = \frac{1}{2} (\mathbf{H} \delta \mathbf{w} - \mathbf{d})^T \mathbf{R}^{-1} (\mathbf{H} \delta \mathbf{w} - \mathbf{d}); \qquad (1)$$

$\mathbf{d} = (\mathbf{d}_0^T, ..., \mathbf{d}_i^T, ..., \mathbf{d}_n^T)^T$ where $\mathbf{d}_i = \mathbf{y}_i^o - H_i[\mathbf{w}^b(t_i)]$ is the innovation vector; H_i is the (possibly nonlinear) observation operator at t_i; and $\mathbf{w}^b(t_i)$ is the background estimate of $\mathbf{w}(t_i)$ obtained by integrating the nonlinear model from t_0 to t_i with $\mathbf{w}^b(t_0)$ as initial condition. The matrix $\mathbf{H} = (\mathbf{H}_0^T, ..., \mathbf{H}_i^T, ..., \mathbf{H}_n^T)^T$ is a concatenated linearized observation operator with $\mathbf{H}_i$ defined such that $H_i[\mathbf{w}(t_i)] \approx H_i[\mathbf{w}^b(t_i)] + \mathbf{H}_i \delta \mathbf{w}(t_i)$ where $\delta \mathbf{w}(t_i) = \mathbf{w}(t_i) - \mathbf{w}^b(t_i)$. In the present study, H_i is linear, and consists of bilinear interpolation on each model level and linear interpolation between model levels. For TAO data, which are available as daily mean values, H_i also includes a time averaging over the 16 time steps that make up a model day. $\mathbf{R}$ is an estimate of the observation-error covariance matrix. Here, the observation errors are assumed to be uncorrelated in space and time so that $\mathbf{R}$ is diagonal; the error variances are set to $(0.5^\circ \text{C})^2$ for TAO data and $(1.0^\circ \text{C})^2$ for all other temperature

data. The formulation of the background-error covariance matrix $\mathbf{B}_{(\mathbf{w})}$ requires careful consideration and will be discussed in detail in the next section.

Note that the choice of the analysis time within the assimilation window is somewhat arbitrary. Here, we define the analysis time to be at t_0 so that the background state $\mathbf{w}^b \equiv \mathbf{w}^b(t_0)$ and the increment $\delta\mathbf{w} \equiv \delta\mathbf{w}(t_0)$. As discussed in Weaver *et al.* (2003), with this definition, the FGAT version of 3D-Var can be interpreted as a limiting case of incremental 4D-Var in which the tangent-linear model that is used to transport $\delta\mathbf{w}(t_i)$ through assimilation window in 4D-Var is replaced by a persistence model $\delta\mathbf{w}(t_i) = \delta\mathbf{w}(t_{i-1})$.

The cost function is minimized iteratively using a gradient descent algorithm. The limited-memory quasi-Newton algorithm M1QN3 (Gilbert and Lemaréchal 1989) is used here with an exact line search to improve its efficiency for quadratic minimization problems. The convergence properties of the minimization are further improved by employing a preconditioning transformation $\mathbf{v} = \mathbf{U}^{-I}\delta\mathbf{w}$ in (1), where $\mathbf{B}_{(\mathbf{w})} = \mathbf{U}\mathbf{U}^T$ and $\mathbf{B}_{(\mathbf{w})}^{-1} = \left(\mathbf{U}^{-I}\right)^T \mathbf{U}^{-I}$, so that $J_b = \mathbf{v}^T\mathbf{v}/2$. The generalized inverse $\mathbf{U}^{-I}$ is needed since $\mathbf{U}$ is rectangular in this study (see section 2.4).

The 3D-Var problem is solved directly in the space of the control vector $\mathbf{v}$, and then transformed back into physical space using the inverse transformation

$$\delta\mathbf{w} = \mathbf{U}\mathbf{v}. \tag{2}$$

Denoting $\mathbf{v}^a$ as the minimizing solution, the analysis increment will be given by $\delta\mathbf{w}^a = \mathbf{U}\mathbf{v}^a$, which in this study will contain increments for both temperature and salinity; $\delta\mathbf{w}^a = (\delta T^a, \delta S^a)^T$. Following Bloom *et al.* (1996), the model state vector is then updated gradually with the analysis increment via a constant 3D forcing term applied to the model equations between t_0 and t_n:

$$\mathbf{x}(t_i) = M(t_i, t_{i-1})[\mathbf{x}(t_{i-1})] + \mathbf{F}\delta\mathbf{w}^a \tag{3}$$

where $M(t_i, t_{i-1})$ is the nonlinear ocean model operator acting on $\mathbf{x} = (\mathbf{u}_h^T, T, S)^T$ between t_{i-1} and t_i, and

$$\mathbf{F} = \frac{1}{n}\begin{pmatrix} 0 & 0 \\ I & 0 \\ 0 & I \end{pmatrix}, \tag{4}$$

I denoting the identity operator and n the number of time steps in the assimilation window.

2.4 Multivariate formulation of $\mathbf{B}_{(\mathbf{w})}$

The spatial and multivariate structure of the analysis increments in a 3D-Var analysis is governed by the formulation of the background-error covariance matrix. To see this, it is sufficient to consider the exact minimizing solution of the 3D-Var problem (1) (Tarantola 1987):

$$\delta\mathbf{w}^a = \mathbf{B}_{(\mathbf{w})} \underbrace{\mathbf{H}^T \left(\mathbf{H}\mathbf{B}_{(\mathbf{w})}\mathbf{H}^T + \mathbf{R}\right)^{-1} \mathbf{d}}_{\delta\widehat{\mathbf{w}}}. \tag{5}$$

In the present study, where only temperature observations are assimilated, the increment $\delta\widehat{\mathbf{w}}$ highlighted by the underbrace in (5) will have nonzero values only for temperature $\delta\widehat{\mathbf{w}} = (\delta\widehat{T}, 0)^T$ and only at those grid-points that are directly influenced by the adjoint of the interpolation operator ($\mathbf{H}^T$). It is thus the application of $\mathbf{B}_{(\mathbf{w})}$ to $\delta\widehat{\mathbf{w}}$ in (5) that is primarily responsible for spatially spreading the observational information. Moreover, $\mathbf{B}_{(\mathbf{w})}$ is

the *only* mechanism by which information can be transferred from the observed (temperature) to the unobserved (salinity) variable.

Our general approach for modelling multivariate constraints in $\mathbf{B}_{(\mathbf{w})}$ follows closely that of Derber and Bouttier (1999). The background-error covariance matrix is defined by

$$
\mathbf{B}_{(\mathbf{w})} = \begin{pmatrix} B_{TT} & B_{TS} \\ B_{ST} & B_{SS} \end{pmatrix} = \begin{pmatrix} E[T'T'^T] & E[T'S'^T] \\ E[S'T'^T] & E[S'S'^T] \end{pmatrix} \tag{6}
$$

where $E[\ ]$ denotes mathematical expectation, and primed variables denote the difference between the background field and the "true" field we wish to estimate (this difference assumed to be unbiased in (6)). The term B_{TT} represents the univariate covariances for T'. Following Weaver *et al.* (2003), we model these $T' - T'$ covariances directly as $B_{TT} = \Sigma_T C_{TT} \Sigma_T$ where Σ_T is a diagonal matrix containing estimates of standard deviations, and $C_{TT} = C_{TT}^{1/2}(C_{TT}^{1/2})^T$ is a symmetric matrix of horizontal and vertical correlations. These univariate correlations are modelled using a diffusion operator (Weaver and Courtier 2001) and are approximately Gaussian. The diffusion operator contains a number of tunable parameters that control the length scales and degree of anisotropy in the correlation functions. The horizontal length scales are taken to be a function of latitude and symmetric about the equator. The zonal and meridional length scales are $8°$ and $2°$, respectively, at the equator, and $4°$ poleward of $20°$N/S, with a linear transition between these values within the equatorial strip. The vertical length scales are taken to be a function of depth, being twice the model's local vertical grid spacing to provide adequate smoothing between model levels. This gives vertical scales of about 20m down to a depth of 100m and increased values below this depth. The background temperature error standard deviations (Σ_T) have been (crudely) approximated by climatology associated with the natural variability of the temperature field in an integration of the model without data assimilation. These values of the correlation parameters and standard deviations are identical to those used in Weaver *et al.* (2003) and Vialard *et al.* (2003).

Substituting (6) into (5), it is clear that when only temperature observations are assimilated, only the first column of $\mathbf{B}_{(\mathbf{w})}$ is used in the computation of the analysis increment. The analysis increment would be influenced by the second column if direct observations of salinity were assimilated or if the application of the observation operator resulted in a transfer of information between temperature and salinity, which would be the case in 4D-Var when implicit in $\mathbf{H}^T$ would be the integration of the adjoint of the tangent linear of the ocean model.

Suppose now that T' and S' can be related through a linear T–S relation of the form $S' = K_{ST}T'$. A discussion of the validity of this assumption and of the precise form attributed to K_{ST} is deferred until the next section. This relation can then be employed directly in (6) to represent the univariate covariances for S' (B_{SS}), and the cross-covariances between T' and S' ($B_{ST} = B_{TS}^T$) in terms of the univariate covariances for T' (B_{TT}):

$$
\mathbf{B}_{(\mathbf{w})} = \begin{pmatrix} B_{TT} & B_{TT}K_{ST}^T \\ K_{ST}B_{TT} & K_{ST}B_{TT}K_{ST}^T \end{pmatrix}, \tag{7}
$$

which can be factored as

$$
\mathbf{B}_{(\mathbf{w})} = \begin{pmatrix} I \\ K_{ST} \end{pmatrix} B_{TT} \begin{pmatrix} I & K_{ST}^T \end{pmatrix} = \mathbf{K} B_{TT} \mathbf{K}^T \tag{8}
$$

where $\mathbf{K} = \begin{pmatrix} I & K_{ST}^T \end{pmatrix}^T$. Derber and Bouttier (1999) refer to $\mathbf{K}$ as a linear "balance" operator. For consistency, we will adopt the same terminology even though, in the current context, the term "conservation" operator may be more appropriate since the T–S relations used to define the operator K_{ST} will be derived from principles of water mass conservation rather than of dynamical balance. In this sense, $\mathbf{K}$ has a much wider meaning and should refer to any (linear) constraint between variables that can be incorporated in the covariance matrix.

From (8) it is clear that $\mathbf{B}_{(\mathbf{w})}$ has rank equal to that of the block matrix B_{TT} and thus is singular. The null-space in $\mathbf{B}_{(\mathbf{w})}$ is associated with "unbalanced" salinity errors; i.e., those errors not described by the balance operator K_{ST}.

This explains why the generalized left inverse ($\mathbf{U}^{-I}$) has been used in the preconditioning transformation defined earlier. From (2), the inverse of the preconditioning transformation is given by $\delta \mathbf{w} = \mathbf{U} \mathbf{v}$ where $\mathbf{U} = \mathbf{K} B_{TT}^{1/2}$ and $B_{TT} = B_{TT}^{1/2} (B_{TT}^{1/2})^T$. Note that while $\delta \mathbf{w} = (\delta T, \delta S)^T$ contains components for both temperature and salinity, $\mathbf{v} = v_T$ contains a single component corresponding to a nondimensional (control) variable for temperature.

By ignoring "unbalanced" errors in salinity (i.e., by setting $S_U' \equiv 0$ where $S' = K_{ST} T' + S_U'$), we are in effect assuming $\mathbf{K}$ to be exact, and treating it as a *strong constraint* in the analysis (Lorenc 2003). This is reflected by the single control variable v_T in the minimization problem. It is possible to introduce $\mathbf{K}$ as a *weak constraint* (e.g., as in Derber and Bouttier (1999)) by prescribing a non-zero variance to the "unbalanced" errors and introducing a new control variable (v_{S_U}) for unbalanced salinity. In the current framework, however, unbalanced salinity variables can effectively be discarded since neither the observations (temperature) nor the 3D-Var observation operator (interpolation) provide information to correct them. The only information to correct salinity comes from the balance operator. The temperature and salinity analysis problems are thus effectively decoupled: a univariate 3D-Var analysis can be performed first to obtain δT^a, and then the balance operator can be applied directly to δT^a to obtain δS^a. Therefore, in the current study, our approach closely resembles the post-analysis correction technique of TH99, and both techniques could be expected to give similar results. Including the T–S relation within the covariance formulation, either as a strong or weak constraint, will have advantages in more general applications, such as combined temperature and salinity data assimilation, as discussed in section 6.2.

3 A state-dependent T–S constraint

3.1 Description of the T–S relation

In this section we wish to design an operator K_{ST} that can explain as much correlation (or "balance") as possible between temperature and salinity. Furthermore, this operator must be linear so that it can be applied within a covariance matrix. Following TH99 and Troccoli *et al.* (2002), we consider a scheme that employs local T–S relationships from the model background state to constrain salinity as a function of temperature.

Suppose that the model background state possesses a well defined T–S relationship so that, at any grid-point, salinity can be expressed as a differentiable function of the background temperature, $S^b = S(T^b)$. For a temperature perturbation T', we can then expand $S(T^b + T')$ in a Taylor series about the background temperature state T^b;

$$S(T^b + T') \approx S(T^b) + \left. \frac{\partial S}{\partial T} \right|_{T=T^b} T'. \tag{9}$$

The salinity perturbation S' resulting from a temperature perturbation T' can thus be defined, to first order, by $S' = \partial S / \partial T |_{T=T^b} T'$. Regions where this relationship is not valid (e.g., in the mixed layer where T and S are weakly correlated) will be considered shortly. To evaluate the derivative in (9), we assume that local temperature and salinity variations occur predominantly through *vertical* displacements of water mass (TH99; Troccoli *et al.* 2002). By the chain rule, we can then approximate the derivative in (9) as

$$\left. \frac{\partial S}{\partial T} \right|_{T=T^b} \approx \left. \frac{\partial S}{\partial z} \right|_{S=S^b} \left. \frac{\partial z}{\partial T} \right|_{T=T^b} \tag{10}$$

where we have neglected the horizontal components of the derivative. From (10) and (9), we can interpret the adjustment of salinity in the inverse of the preconditioning transformation as follows. On each iteration of the minimization process, a new value of the control variable v_T is estimated and converted into a temperature perturbation $T' = \Sigma_T C_{TT}^{1/2} v_T$. Using the local gradient of the background T profile, this temperature perturbation

is then transformed linearly into an equivalent depth-dependent vertical displacement of the profile: $(\Delta z)_T = \partial z/\partial T|_{T=T^b} T'$. Then, using the local gradient of the background S profile and the vertical displacement vector $(\Delta z)_T$, a salinity perturbation $S' = \partial S/\partial z|_{S=S^b} (\Delta z)_T$ is computed, and used along with T' in the evaluation of the cost function and its gradient for the next iteration of the minimization. The vertical derivatives are computed numerically using centred finite differences applied directly to the background T and S fields. This procedure gives an estimate of the vertical derivative at the midpoint between T (and S) points. The derivatives at successive midpoints are then averaged to give an estimate of the vertical derivative directly at T (and S) points.

Water mass T–S properties are largely preserved in regions where isentropic processes dominate (e.g., in the tropical thermocline) and hence we can expect a T–S constraint to be beneficial there. Where nonisentropic processes are important, for example in the mixed layer, temperature and salinity variations are uncorrelated and we should avoid applying a T–S constraint. To account for this possibility, we introduce a multiplicative parameter α in the T–S relation such that

$$S' = \alpha \left. \frac{\partial S}{\partial T} \right|_{T=T^b} T' = K_{ST} T' \tag{11}$$

where $K_{ST} = \alpha \, \partial S/\partial T|_{T=T^b}$. For simplicity, α is set to either zero or one, depending on various conditions in the background state. To take into account the weak correlation between T and S in the mixed layer, we set α to zero in regions where the background vertical mixing coefficient A_v^b is strong ($A_v^b > 5 \times 10^{-4} \, \mathrm{m}^2 \, \mathrm{s}^{-1}$). Temperature and salinity are also expected to be weakly correlated in regions where temperature is well mixed but salinity is strongly stratified (e.g., in the *barrier layer*; Lukas and Lindström 1991). Setting α to zero when $(\partial S/\partial z|_{S=S^b})/(\partial T/\partial z|_{T=T^b}) > 1 \, \mathrm{psu} \, (^\circ\mathrm{C})^{-1}$ was found to be sufficient to eliminate spurious salinity increments arising under such conditions.[2] To avoid numerical problems in computing (10) in regions of weak temperature stratification, we also set $\alpha = 0$ when $\partial T/\partial z|_{T=T^b} < 10^{-3} \, {}^\circ\mathrm{C} \, \mathrm{m}^{-1}$. Finally, a local two-grid point Shapiro filter was used to smooth K_{ST} in each model level.

It is important to note the strong dependence of K_{ST} on the background state, both through the parameter α and the derivative $\partial S/\partial T$. This state dependency in K_{ST} implies that, in a cycling 3D-Var system, the T–S constraint will evolve from one cycle to the next and thus will implicitly take into account the impact of the data assimilation from previous cycles in deriving the background salinity error covariances for the current cycle.

3.2 Reconstructing a density profile from temperature observations: a twin experiment

In this section we perform an identical twin experiment to illustrate the impact of the T–S constraint in 3D-Var when only temperature "data" are assimilated. For simplicity, we consider the problem of reconstructing a density profile using "data" sampled from the corresponding temperature profile at different depths. The synthetic data were extracted from a "true" state taken to be the model restart on 1 January 1993 (see section 2.1). The background state for the twin experiment was taken from a model restart obtained by spinning up the model using different surface forcing fields (the same ones used by Weaver *et al.* (2003)).

The temperature "observations" were extracted at 11 different depths (between 0 and 500m) from a profile located at 160° E on the equator. No noise was added to the "observations". Figure 1 shows the temperature and salinity increments produced by 3D-Var and the corresponding "true" increments defined as the difference

---

[2]Rather than parametrising α as an empirical function of the background state, we could have used a statistical parametrisation in which α is computed by linear regression between appropriate difference fields of T and S. Such a regression analysis was performed using an ensemble of difference fields produced with perturbed wind-stress and SST fields, and the results from that analysis were in good agreement with our simple parametrisation of α.

between the background and "true" profiles. The temperature analysis increment is in quite good agreement with the "true" increment, although it underestimates the amplitude of the increment particularly near the maximum and base of the thermocline, as well as in the mixed layer (Fig. 1a). The salinity analysis increment computed using the T–S constraint gives a good estimate of the "true" salinity increment below the mixed layer, although it slightly underestimates its amplitude in the lowest part of the thermocline (Fig. 1b). This could be linked to deficiencies in the T–S scheme but also to deficiencies in the temperature analysis itself as noted above. Within the mixed layer (above 70m), the analysed salinity increment is zero since the T–S constraint is not applied there. Figure 1b suggests that it may be desirable to extrapolate the balanced salinity increment at the base of the mixed layer directly to the surface (as illustrated by the dotted line in Fig. 1b) in order to avoid a discontinuity there. While this is an interesting possibility, we have not explored it in the experiments that are presented in the remainder of the paper.

Note that similar twin experiments were performed at different locations and times and the results were qualitatively similar to those illustrated in Fig. 1.

4 The ocean analyses

4.1 The assimilation experiments

Two sets of 3D-Var experiments are performed using *in situ* temperature data. One (TS) uses the T–S constraint in **B** to produce a multivariate analysis of temperature and salinity on each assimilation cycle, whereas the other experiment (NOTS) does not use this constraint and thus produces a univariate analysis of temperature on each cycle. The assimilation window is 10 days in both experiments. A third experiment (CTL) does not assimilate data and will be referred to as the control run. The experiments are run over a 6-year period from 1 January 1993 to 31 December 1998 with the surface forcing fields described in section 2.1.

4.2 Impact of the new forcing on the mean state

The reason for adopting the new forcing strategy compared to that used by Vialard *et al.* (2003) was to provide a better constraint on the upper ocean salinity content. Figure 2 shows the average salinity in the upper 50m of the TAO region ($160°\text{E} - 70°\text{W}; 10°\text{S} - 10°\text{N}$) for the univariate 3D-Var experiment (EX3D) presented in Vialard *et al.* (2003) and for NOTS which is a similar experiment except that it uses the new surface forcing fields. Note that the two experiments also start from slightly different initial conditions as they have been produced using different "spin-up" strategies. While the upper ocean salinity does not seem to display a significant drift in NOTS, it decreases by 0.4 psu by the end of the 6-year assimilation period in EX3D, suggesting that the new strategy for the fresh water forcing improves the quality of the upper ocean salinity field.

Another important modification of the forcing is the use of the ERS-TAO wind stress product (see Sec. 2.1). The difference between the 1993-98 average zonal wind stress in ERS-TAO and its ERS counterpart (not shown) is negative over most of the TAO region, indicating that the easterlies are associated with stronger zonal wind stresses in the ERS-TAO product. This difference reaches 0.02 N.m^{-2} locally in the east Pacific which represents between 10-30% of the mean wind stress. Figure 3 illustrates the impact of this stronger wind product on the zonal surface currents. As already discussed by Vialard *et al.* (2003), the univariate 3D-Var using the ERS forcing displays an eastward surface current bias at the equator in the central and eastern part of the basin (Fig. 3a). Bell *et al.* (2004) have suggested that this current bias could be linked to an imbalance that develops between the prescribed wind stress and the zonal pressure gradient when the latter is constrained by assimilated temperature observations. Indeed, if the prescribed easterlies are too weak and the zonal thermal

gradient is constrained to be close to the observed gradient, the resulting pressure field will tend to accelerate the currents eastward. Since ERS-TAO wind stress has a systematically stronger zonal component than the ERS wind stress, the results from NOTS and EX3D would seem to confirm this explanation. In NOTS, the eastward surface current bias at the equator is reduced by 0.2m.s^{-1} (Fig. 3b).

4.3   Impact of the T–S constraint on the temperature and salinity mean state

In this section the set of analyses (CTL, NOTS and TS) is examined to assess the impact of the T–S constraint on the model temperature and salinity mean state. The 1993-98 average temperature from TS and NOTS are very similar (not shown); applying the T–S constraint does not significantly change the temperature analysis. In both experiments the main impact of the assimilation of temperature data is to tighten the thermocline by adding colder water below it and warmer water above it (Vialard *et al.* 2003).

Vertical equatorial sections of the 1993-98 average salinity in the upper 300m of the ocean are shown in Fig.4 for the Levitus climatology, the two assimilation experiments (TS, NOTS) and the control (CTL). The Levitus climatology (Fig. 4a) is our observational reference. In general, the three experiments reproduce the main salinity structures of Levitus. However, in NOTS, the salinity maximum around 150m in the west of the basin is reduced to 35.0 psu compared to 35.2 psu in Levitus, CTL and TS. This bias is the result of the univariate assimilation of temperature since it does not appear in CTL, and is in agreement with Vialard *et al.* (2003) who showed a decrease in the upper ocean salinity content in their univariate 3D-Var experiment (EX3D). In TS, where a T–S constraint is applied, this bias disappears and the maximum pattern is restored.

The mean 1996 salinity profiles between 0 and 2000m for TS, NOTS and CTL are shown in Fig. 5. CTL is in good agreement with Levitus especially below 500m. In NOTS, however, the water is too fresh above 400m and too salty below (this is also evident in Fig. 4). This is consistent with Troccoli *et al.* (2002) who showed that spurious mixing can freshen the upper ocean and increase salinity in the deep ocean as a result of univariate temperature assimilation. In both TS and the experiment of Troccoli *et al.* (2002), the mean salinity profile is improved when the salinity constraint is applied. The T–S constraint prevents the artificial freshening and saltening above and below 400m, respectively.

Figure 6 displays the evolution of the monthly salinity content in the upper 300m in the TAO region. After 6 years, the upper ocean salinity content in NOTS has decreased by 0.2 psu, this decrease being strongest in the first two years of the experiment. This salinity drift is a particular aspect of the univariate 3D-Var analysis since it does not appear in CTL and is largely corrected for in TS. TS still displays some differences from the Levitus value (up to 0.1 psu). The salinity variability in TS, as well as in CTL, is difficult to validate in the absence of interannual observations of the salt content. However, it seems to be too large to be realistic, being equivalent to a change in precipitation of 1.1 mm/day during two years over the whole TAO region.

4.4   Comparison to independent salinity observations

The comparisons above are only qualitative since the Levitus and model climatologies are not representative of the same period. We now make a more quantitative validation of the model salinity fields by comparing them to the (non-assimilated) salinity observations of Johnson *et al.* (2002) (section2.2). The comparison was done by computing the difference between the model background salinity field and the data at their precise measurement time and location using the 3D-Var observation operator. These differences will be referred to as the background-minus-observation (BmO $\equiv H_i(\mathbf{x}_i^b) - \mathbf{y}_i^o$)).

Figures 7b and c present, respectively, the 1993-98 average and standard deviation of the BmO over the TAO region from CTL, NOTS and TS. For reference, the average of the observed salinity profile in the upper 500m

of the water column is also shown (Fig. 7a). In the upper 100m, there is no clear improvement in TS with respect to NOTS in either the mean or standard deviation. This could be expected since the T–S constraint is not applied in the mixed layer, and thus can not directly affect salinity there. In this region, CTL is in better agreement with salinity observations than either TS or NOTS. Between 100m and 250m, there is much better agreement with the salinity observations in TS than in NOTS, as can be deduced from the smaller standard deviation and absolute average of the BmO. This confirms quantitatively the improvement of the subsurface salinity structure already illustrated qualitatively in section 4.3. Below 250m, of the three experiments, TS displays the smallest standard deviation of the BmO, while CTL the smallest mean of the BmO.

Figure 8 shows the average and standard deviation of the BmO in the upper 300m of the TAO region as a function of time. This figure shows that the average improvement due to the T–S constraint seen in Fig. 7 is also true at almost any time during the experiment. In both Figs. 7 and 8, the average of the BmO exhibits a clear positive and negative salinity bias in CTL and NOTS, respectively (Fig. 8a). At most times, TS displays smaller average and standard deviation of the BmO than those in NOTS. The standard deviation of the BmO for CTL is slightly smaller than that of TS (as in the top half of Fig. 7c). This suggests that the variability of the salinity content in CTL is slightly better than in the assimilation experiments.

By comparing with independent salinity observations, we have thus shown that, when assimilating only temperature observations, there is a clear improvement in the mean and variability of the salinity field when the T–S constraint is applied, but no obvious improvement over the control experiment in which no data are assimilated.

4.5   Impact of the T–S constraint on the mean circulation

Figure 9 shows the 1993-98 zonal surface current for TS. It can be seen in Fig. 9 that the spurious equatorial eastward currents of NOTS (Fig. 3b) are eliminated in TS. Figure 10 shows vertical profiles of the zonal currents from CTL, NOTS and TS compared to current data at three equatorial TAO moorings (at 165°E, 140°W and 110°W). There is good agreement between TAO and CTL except near the maximum of the undercurrent which is underestimated in CTL. At 140°W the surface currents in TS are improved compared to those in NOTS (Fig. 10b). However, the intensity of the undercurrent maximum in the central and eastern Pacific is not as well captured in TS as in NOTS. Both TS and especially NOTS display too large eastward currents below the core of the undercurrent at 140°W and 110°W which are probably associated with large vertical velocities below the thermocline in both experiments (Figs. 11b and c).

Figure 12 allows us to diagnose the origin of the current differences between TS and NOTS. It displays the 170°W-120°W zonally averaged difference between TS and NOTS for mean temperature, salinity, dynamic height and the zonal velocity fields (Fig. 12a-d). Also displayed is the geostrophic component of the zonal current (Fig. 12e) which has been computed directly from the dynamic height difference in Fig. 12c using a combined f-plane and β-plane solution (Picaut and Tournier 1991). The differences in zonal currents between TS and NOTS are seen to be reasonably well approximated by geostrophy. The dynamic height (and thus current) differences are predominantly explained by the salinity differences in Fig. 12b. The eastward bias in NOTS can be related to the erosion of the subsurface salinity maximum close to the equator (between 2°S-5°N and 50-150m in Fig. 12b) in NOTS which causes a depression in dynamic height in the upper 100m (Fig. 12c) and thus, because of the weak value of the Coriolis parameter there, a relatively strong eastward surface current anomaly of up to 20cm.s^{-1}. The better preservation of the salinity structure in TS prevents the development of this spurious current. Similar processes are involved to explain the differences between TS and NOTS below the core of the undercurrent, between 150m and 400m near 2.5°S, in Fig. 10c. In this case, it is rather the subsurface salinity changes south of 5°S between 100-200m in Fig. 12c that lead to the current differences.

5   Heat and fresh water budgets

In this section the heat and fresh water budgets in CTL, NOTS and TS are investigated. The analysis of these budgets will allow us to understand how the extra heat and salt sources associated with the analysis increment act to change the dynamical balances in the model. Details on how the heat and fresh water budgets are computed are given in the Appendix.

5.1   Temperature budget

Figure 13 shows the 1993-98 average contribution to the total heat budget at the equator of zonal and vertical advection, vertical diffusion and the temperature analysis increment for CTL, TS and NOTS (see Eq. (17) in the Appendix). Lateral diffusion and meridional advection do not contribute significantly to the average heat budget and are therefore not shown.

In CTL, the balance is representative of the thermocline equilibrium close to the equator. The zonal flow associated with the undercurrent carries warm water eastward, which results in a positive zonal advection term in the thermocline region (Fig. 13a) that is largely balanced by upwelling of deep cool water by equatorial upwelling (Fig. 13b). These two contributions compensate to maintain the thermocline. In the eastern Pacific, where the thermocline is close to the surface, the influence of mixing becomes important (Fig. 13c). There, vertical diffusion tends to cool the surface and warm the subsurface.

This balance is modified in the presence of data assimilation since there is now an extra term in the heat budget coming from the heat added or removed by the analysis increment (see Appendix). In NOTS, the basic balance in the thermocline described above largely holds: warming by zonal advection, cooling by equatorial upwelling and vertical redistribution of heat by mixing in the eastern part of the basin. However, most of the terms become notably stronger in the presence of data assimilation. Compared to CTL, the thermocline is tighter both in NOTS and TS which results in larger horizontal and vertical temperature gradients. The undercurrent is strongly intensified in NOTS compared to CTL (Fig. 10). This results in a larger (and probably better) estimate of the zonal advection term which is largely balanced by an equivalent increase of cooling by vertical advection (in turn linked to the vertical gradients and equatorial upwelling which are both stronger in NOTS and TS than in CTL as shown in Fig. 11). The increase in vertical mixing in the eastern Pacific is probably a result of both a tighter thermocline and spurious mixing in the assimilation experiments (Troccoli *et al.*, 2002, Vialard *et al.*, 2003). These contributions to the heat budget do not compensate as in CTL, thus resulting in local imbalances which are compensated by the analysis increment (Fig 13g). The increment in NOTS has locally large values, with systematic warming or cooling of up to 3°C.month^{-1}. The spatial structure of the increment can be recognized in parts of the vertical advection term (e.g., the strong cooling between 100-250m around 175°W). At these locations, the assimilation leads to an unrealistic increase of the vertical current close to the equator (Fig. 11b). Figure 13 illustrates that this in turn leads to an increase in vertical advection which is perpetually counterbalanced by the analysis increment. As discussed in Vialard *et al.* (2003), the assimilation in a univariate 3D-Var continuously acts to correct for a bias of its own making. More generally, the assimilation compensates for any imbalance in the heat budget. For example, this is the case between 100-150m at 140°W or at the surface in the eastern part of the basin where the origin of the imbalance is a combination of spurious zonal and vertical advection.

With the introduction of the T–S constraint the zonal advection term is reduced overall compared to that in NOTS (cf. Figs. 13d and h) and the vertical advection term is locally reduced where the salinity increment is large (cf. Figs. 13e and i). The thermocline structure is similar in both TS and NOTS suggesting that these reductions are the result of a weaker undercurrent (Fig. 10) and a weaker vertical current in TS (Fig. 11c). A

positive feature of TS is that the mean temperature increment is reduced, indicating that the tendency of the assimilation system to produce a temperature bias through a spurious circulation has been reduced. The T–S constraint thus not only provides a better salinity state as illustrated in section 4.3, but it also results in a better balance between terms in the temperature budget. It is also interesting to note that there is no significant change in the vertical mixing term between TS and NOTS, a point we will come back to in the next section.

5.2 Salinity budget

We now investigate the salinity budget to assess how the salinity increment is acting to prevent salinity biases from developing in TS. Figure 14 shows the main contributing terms to the salinity budget at the equator for CTL, NOTS and TS. The largest terms are found close to the surface where the salinity gradients are strongest; in the temperature budget, they were found in the thermocline.

In CTL, the main equilibrium in the near surface layer is between horizontal (zonal plus meridional) advection (Fig. 14a), vertical advection (Fig. 14b) and vertical mixing (Fig. 14c). Zonal advection carries fresh water westward close to the surface. This is in agreement with Vialard *et al.* (2002) who showed that this westward fresh water transport is due to both advection by the mean currents and transport by tropical instability waves. Equatorial upwelling (Fig. 11) combined with a negative salinity gradient between the surface and 100m results in a salting above the subsurface salinity maximum (Fig. 14b). Finally, vertical mixing (Fig. 14c) tends to increase salinity in the fresh layer close to the surface, and freshen water in the region of the subsurface salinity maximum.

In NOTS, the biggest change in the zonal advection term (Fig. 14d) is in the subsurface central Pacific. It is probably the much stronger undercurrent in NOTS in this region that leads to a stronger estimate of zonal advection in this region. Salty water is advected from the maximum salinity region towards the east between 100-150m. The upwelling below 100m in NOTS (Fig. 11b), and thus below the subsurface salinity maximum, leads to a strong freshening between 100-200m through vertical advection (Fig. 14e). The weakening of the subsurface salinity maximum that was seen in Fig. 4 also leads to a decrease in the upward advection of salt in the central Pacific between the surface and 100m. At this depth, the vertical velocity is similar to that of CTL so that the change in vertical advection is due to the smaller magnitude of the vertical salinity gradient than that of CTL. Despite a noticeable increase in the magnitude of the vertical mixing coefficients in NOTS (not shown; see Fig. 8 in Vialard *et al.* (2003)), vertical diffusion is smaller in NOTS than in CTL because of the weakened salinity stratification in NOTS.

The terms of the salt budget are quite similar in TS and NOTS. However, the eastward advection of salt by the undercurrent and the subsurface freshening by spurious upwelling are stronger in TS. Since both the undercurrent and the spurious upwelling below 100m are weaker in TS than in NOTS, this is due to the stronger and better preserved salinity gradients in TS. It was seen earlier that the subsurface salinity maximum is better maintained in TS because there is a salinity increment that can act to compensate for the salt advection by unrealistic currents. Indeed, the salinity increment (Fig. 14j) has locally similar structures to those that appear in the zonal and vertical advection terms (Fig. 14g and h).

The description above is useful to understand how, in the stationary regime, the assimilation increment acts to compensate for imbalances between the physical terms of the salt budget. However it does not allow us to analyse the reasons for the salinity drift that was seen in Fig. 6. Figure 15 shows the time-integrated terms of the salinity equation over the upper 300m of the TAO region (see Eq. (19) in the Appendix). The vertical diffusion term has been split into the effect of surface forcing and the contribution from diffusive fluxes at 300m (see Eq. (20)). In CTL (Fig. 15a) the change in salinity is mainly caused by surface forcing and advective effects. Horizontal diffusion contributes to a lesser extent, as a small but steady saltening term. These terms largely

compensate each other, thus leading to a weak change of the upper 300m salt content over the 1993-98 period (Fig. 6). In NOTS (Fig. 15b) the relative balance of terms in the salt budget is significantly different and results in the relatively large drift of -0.2 psu by the end of the period shown in Fig. 6 and by the dashed curve in Fig. 15b. This is essentially due to a change in the advective terms which causes a strong freshening that is only partially compensated by the flux correction technique used in the fresh water surface forcing. This could be expected since the flux correction technique only has a significant impact near the surface. (Note that the use of flux correction implies that the fresh water forcing is different in CTL and NOTS). Lateral diffusion does not change much between NOTS and CTL. On the other hand, the diffusive flux at 300m, which was very weak in CTL, is now somewhat stronger and contributes to a 0.05 psu freshening over the whole period. Troccoli *et al.* (2002) invoked spurious mixing caused by static instabilities as the main cause of upper ocean freshening in a univariate assimilation experiment similar to NOTS. The analysis above shows that the main cause of the freshening in NOTS is actually a change in advection, and that spurious mixing contributes to a much lesser extent. This difference may be partly linked to the absence of a vertical smoothing mechanism in the OI system of Troccoli *et al.* (2002), which could result in rather abrupt changes in the temperature field between levels and thus exacerbate the problem of artificial instabilities.

In TS the salinity drift over the whole period is significantly reduced (Fig. 15c). Compared to CTL, the only terms that change significantly are the surface forcing (due to the flux correction approach) and lateral diffusion, both of which contribute to a saltening that is largely balanced by the salinity increment. Whereas there was a strong change in advection in NOTS which lead to a strong freshening of the upper ocean, the advective term in TS is qualitatively similar to that of CTL. This is in agreement with section 4.5 which showed that the circulation was significantly improved in TS. The weak freshening of the upper layer by increased vertical mixing seen in NOTS is also noticeably reduced in TS.

6   Summary and discussion

6.1   Summary

Previous studies (Troccoli *et al.* 2002; Burgers *et al.* 2002; Vialard *et al.* 2003) have illustrated the importance of multivariate constraints to avoid generating spurious features in the tropical ocean salinity and current fields when assimilating subsurface temperature data. In this study, we have presented a general framework for introducing multivariate constraints in the background-error covariance matrix of variational data assimilation. Specifically, this framework was used to introduce a T–S constraint in the ocean 3D-Var system of Weaver *et al.* (2003). Following Troccoli and Haines (1999), the T–S constraint was defined by a local T–S relation derived from the model background state at the beginning of each assimilation cycle. A procedure was defined for linearizing the T–S relation so that it could be included as a constraint within the covariance matrix. By linearizing about the background state, the T–S constraint was made state dependent and thus implicitly could account for time variations in the local T–S relation.

An idealized single-profile experiment illustrated qualitatively how the method can reconstruct a salinity profile from temperature measurements. Three experiments were then performed over the 1993-98 period: a control run without data assimilation, and two 3D-Var experiments with and without the T–S constraint. In both 3D-Var experiments, *in situ* temperature data from the GTSPP were assimilated using a 10-day window. The incremental updating procedure of Bloom *et al.* (1996) was then used to correct the model fields with the analysis increment. With the T–S constraint, the 3D-Var analysis was multivariate in temperature and salinity. Without the T–S constraint, the 3D-Var analysis was strictly univariate in temperature.

Comparing the two 3D-Var experiments showed that the T–S constraint significantly improved the salinity field.

This improvement in salinity complemented the improvement in temperature which was similar in both assimilation experiments. The subsurface salinity maximum, which was strongly eroded in the univariate experiment, was better preserved when the T–S constraint was applied. Comparison to independent salinity observations confirmed that the salinity structure was improved, both on average and at most times during the experiments. However, the salinity variability in the multivariate experiment was slightly degraded relative to the control. The introduction of the T–S constraint also improved the ocean currents in the assimilation experiments. For example, it eliminated a large eastward bias in the surface currents in the central and eastern Pacific which was present in the univariate experiment. A similar current bias has also been observed in other univariate assimilation studies and has been loosely attributed to a general "balance" problem arising from univariate assimilation near the equator (Burgers *et al.* 2002; Vialard *et al.* 2003; Bell *et al.* 2004). In this study it was shown that this bias was associated with eastward geostrophic currents that were generated because of an erosion of the salinity maximum. In the multivariate experiment, the T–S constraint was able to restore the salinity maximum and thus reduce these artificial geostrophic currents.

Analysis of the heat and salt budgets in the various experiments allowed us to examine how the assimilation changed the term balances in the model. In the univariate experiment, the assimilation created a spurious circulation that perpetually degraded the model thermal structure. On each assimilation cycle, the analysis increment was then forced to counteract this problem by correcting the temperature bias that was inflicted by the assimilation in the previous cycles. When the T–S constraint was applied, the spurious circulation was reduced and the mean temperature increment decreased, suggesting that less work had to be done by the assimilation to correct for the bias of its own making. While the spurious currents were reduced in the multivariate experiment, they were still present and tended to degrade the salinity field. In the multivariate experiment, the salinity increment could compensate for this bias and thereby maintain the salinity structure, in a similar way that the temperature increment could compensate for a related bias in the temperature field.

The analysis of the mean upper ocean salt budget as a function of time allowed us to identify unrealistically strong advection in the univariate experiment as the main cause of the salinity drift which lead to a strong freshening of the upper ocean. In the multivariate experiment, the advection term was restored to a level comparable to that of the control run, and as a result the salinity drift was significantly reduced. It is interesting to contrast this explanation to that of Troccoli *et al.* (2002) who suggested enhanced vertical mixing resulting from univariate temperature assimilation as the main reason for the erosion of the salinity maximum (and hence freshening of the upper ocean). Vertical mixing was shown to be strong in the univariate experiment but not the dominant factor. Indeed, the improvement seen in the surface currents when the T–S constraint was applied cannot be explained by a reduction of vertical mixing since this would not affect the overall heat and salt content of the water column and thus would lead to only a small change in sea level and surface currents.

6.2 Discussion

One of the main objectives of this study was to illustrate how the nonlinear salinity adjustment method of Troccoli and Haines (1999) could be cast within the framework of variational data assimilation. A distinguishing feature of our approach was the use of a *linearized* T–S constraint within a "balance" operator of the background-error covariance matrix. Since the balance operator acts on increments generated during the minimization process, the linear assumption would not appear to be a particularly restrictive one, providing the increments are "small". Since the improvements to our analyses were qualitatively similar to those documented in Troccoli *et al.* (2002), we suspect that the errors induced by linearization were minor in this study. The linear assumption may break down, however, if the increments are large in which case a relinearization of the balance operator about a recent estimate of T and S obtained during minimization may be desirable to improve the approximation.

While many aspects of the ocean analysis have been significantly improved with the inclusion of the T–S constraint, various problems remain. For example, the near-surface salinity is degraded relative to both the control and univariate experiments (Fig. 7), zonal and vertical currents below the thermocline are far too strong (Figs. 10 and 11, and vertical mixing coefficients are abnormally large (not shown). These findings suggest that further improvements to the assimilation system are necessary.

The increased errors in the near-surface salinity may be partly related to the discontinuity in the T–S constraint at the base of the mixed layer, where it is set to zero. Rather than applying no constraint on salinity between the base of the mixed layer and the surface, it may be beneficial to extrapolate the salinity balance just below the mixed layer directly up to the surface. This would be a straightforward extension of the method which should be tested. The analysis of the salinity field could obviously be improved through the direct assimilation of salinity data from, for example, Argo floats and CTDs. The general strategy adopted in this study for modelling T–S constraints in the covariance operator makes it straightforward to assimilate salinity data in combination with temperature data, and thus to create a two-way flow of information between temperature and salinity. Better use of salinity data could be made by using weak constraint versions of the T–S constraint so that "balanced" covariances can be given less weight relative to "unbalanced" covariances in regions where T–S relationships are weak. These extensions would require careful tuning of the covariance statistics of the unbalanced component of the background salinity error to achieve an appropriate partition of the covariances into balanced and unbalanced components.

Our multivariate formulation of the background-error covariance matrix gives a critical role to the covariance statistics of (balanced) temperature for establishing the balanced part of the covariance matrix for salinity. Improvements in the specification of the temperature error covariances would thus translate into improvements in the analysis of salinity as well as temperature. There is considerable scope for improving these covariance estimates. For example, the climatological variances that were used for the background errors are probably too large and too broadly spread out over the upper ocean. This may induce increments that are too large below the thermocline and be partly responsible for the overly strong vertical mixing and vertical velocities seen there. A better representation of the variances would take into account the local stratification of the thermocline so that the larger variances can be properly focussed in regions where the local variability is strongest. One way to achieve this is to parametrise the variances in terms of the vertical gradient of the background temperature state. Improvements to the velocity field can also be expected by extending the balance operator to include geostrophic constraints (Burgers *et al.* 2002), thereby creating a fully multivariate 3D-Var analysis that can simultaneously correct all state variables (temperature, salinity and velocity) from any single data-type. Recent 3D-Var sensitivity experiments with these new developments have indeed resulted in a noticeable decrease in the magnitude of the vertical velocities and improvement in the zonal currents. These developments to the covariance matrix can also be expected to have a positive impact in 4D-Var.

Acknowledgements

Appendix: Computing the heat and salt budgets

One of the objectives of this study is to understand how the extra heat and salt sources associated with the temperature and salinity increments influence the term balances in the prognostic equations for temperature and salinity. Taking into account the analysis increment, the temperature equation can be written as

$$\frac{\partial T}{\partial t} = -\mathbf{u}_h \cdot \nabla T - w\frac{\partial T}{\partial z} + D_h(T) + \left(\frac{Q_s}{\rho_0 C_p}\right)\frac{\partial b}{\partial z} + \frac{\partial}{\partial z}\left(A_v^T\frac{\partial T}{\partial z}\right) + F\,\delta T^a \tag{12}$$

where ∇ is the horizontal gradient operator, w is the vertical velocity, D_h is the horizontal diffusion operator, Q_s is the penetrative solar heat flux, $b(z)$ is the fraction of solar heat flux that reaches the depth z, ρ_0 is a constant reference density of sea water, C_p is the specific heat of sea water, A_v^T is the vertical diffusion coefficient, δT^a is the temperature increment, and F is a weighting function defined such that over each 10-day assimilation cycle

$$\int_{1\,\text{cycle}} F\,dt = 1. \tag{13}$$

All other symbols in (12) have been defined previously in section 2.3. The surface boundary condition for T is

$$\left(A_v^T\frac{\partial T}{\partial z}\right)_{z=0} = \frac{Q^*}{\rho_0 C_p} \tag{14}$$

where Q^* is the non-penetrative part of the total surface heat flux.

The salinity equation can be written as

$$\frac{\partial S}{\partial t} = -\mathbf{u}_h \cdot \nabla S - w\frac{\partial S}{\partial z} + D_h(S) + \frac{\partial}{\partial z}\left(A_v^T\frac{\partial S}{\partial z}\right) + F\,\delta S^a \tag{15}$$

where δS^a is the salinity increment. The surface boundary condition for S is

$$\left(A_v^T\frac{\partial S}{\partial z}\right)_{z=0} = (e-p)S_{z=0} \tag{16}$$

where $e-p$ denotes the fresh water (evaporation-minus-precipitation) forcing and $S_{z=0}$ the sea surface salinity.

Integrating (12) and (15) over the 1993-98 period, it is possible to diagnose the relative contributions of the different terms to the changes in heat and salt:

$$\theta_{\text{end}} - \theta_{\text{start}} = Ah(\theta) + Az(\theta) + Dh(\theta) + Dz(\theta) + \sum_{\text{all cycles}} \delta\theta^a \tag{17}$$

where $\theta = T$ or S, and $Ah(\theta), Az(\theta), Dh(\theta)$ and $Dz(\theta)$ represent the time-integrated values of horizontal (zonal + meridional) advection, vertical advection, horizontal diffusion and vertical diffusion, respectively, and θ_{start} and θ_{end} are the temperature or salinity states at the start (1 January 1993) and end (31 December 1998) of the assimilation period. Note that $Dz(\theta)$ includes the contributions from both the penetrative solar heat flux (for $\theta = T$) and the surface forcing fluxes (Eqs. (14) and (16)).

Introducing the area (Σ) and volume (V) averaging operators

$$\left(\overline{\overline{\bullet}}\right) = \frac{1}{V}\int_{V'} (\bullet)\,dV' \qquad\qquad \left(\overline{\bullet}\right) = \frac{1}{\Sigma}\int_{\Sigma'} (\bullet)\,d\Sigma' \tag{18}$$

where $V = \Sigma \times H$ (area $\times$ depth), we can define the volume average of the terms in (15) as

$$\frac{\partial \overline{\overline{S}}}{\partial t} = \overline{\overline{Ah(S)}} + \overline{\overline{Az(S)}} + \overline{\overline{Dh(S)}} + \overline{\overline{Dz(S)}} + \overline{\overline{F \, \delta S^a}}. \tag{19}$$

In this study we are interested in computing (19) over the three-dimensional TAO region: $160^{\circ}\,\mathrm{E} - 70^{\circ}\,\mathrm{W}; 10^{\circ}\,\mathrm{S} - 10^{\circ}\,\mathrm{N}; 0 - 300\mathrm{m}$. For vertical diffusion, the volume integral can be simplified as

$$\begin{aligned}
\overline{\overline{Dz(S)}} &= \frac{1}{V} \int_{V'} \frac{\partial}{\partial z} \left(A_v^T \frac{\partial S}{\partial z} \right) \, dV' \\
&= \frac{1}{\Sigma H} \int_{\Sigma'} \left[A_v^T \frac{\partial S}{\partial z} \right]_{z=-H}^{0} d\Sigma' \\
&= \frac{1}{H} \left[\overline{(e-p)\, S_{z=0}} - \overline{A_v^T \frac{\partial S}{\partial z}}\Big|_{z=-H} \right]
\end{aligned} \tag{20}$$

where $\overline{(e-p)S_{z=0}}$ is the average fresh water flux entering the TAO box at the surface, and $\overline{A_v^T \, \partial S/\partial z}\big|_{z=-H}$ is the average salinity flux diffused at the bottom of the TAO box ($H = 300\mathrm{m}$).

REFERENCES

Bell, M. J., M. J. Martin and N. K. Nichols, 2004: Assimilation of data into an ocean model with systematic errors near the equator. *Q. J. Roy. Meteor. Soc.*, **130**, 873–893.

Bloom, S. C., L. L. Takacs, A. M. Da Silva and D. Levina, 1996: Data assimilation using incremental analysis updates. *Mon. Wea. Rev.*, **124**, 1256–1271.

Burgers, G., M. Alonso Balmaseda, F. C. Vossepoel, G. J. Van Oldenborgh and P. J. Van Leeuwen, 2002: Balanced ocean-data assimilation near the equator. *J. Phys. Oceanogr.*, **32**, 2509–2519.

Cooper, N. S., 1988: The effect of salinity in tropical ocean models. *J. Phys. Oceanogr.*, **18**, 697–707.

Derber, J. C. and F. Bouttier, 1999: A reformulation of the background error covariance in the ECMWF global data assimilation system. *Tellus*, **51A**, 195–221.

Derber, J. and A. Rosati, 1989: A global oceanic data assimilation system. *J. Phys. Oceanogr.*, **19**, 1333–1347.

Gilbert, J.-C. and C. Lemaréchal, 1989: Some numerical experiments with variable storage quasi-Newton algorithms. *Math. Programming*, **45**, 407–435.

Huffman, G. J., R. F. Adler, P. Arkin, A. Chan, R. Ferraro, A. Gruber, J. Janowiak, A. McNab, B. Rudolf and U. Schneider, 1997: The Global Precipitation Climatology Project (GPCP) combined precipitation dataset. *Bull. Amer. Met. Soc.*, **78**, 5–20.

Ide, K., P. Courtier, M. Ghil and A. C. Lorenc, 1997: Unified notation for data assimilation: Operational, sequential and variational. *J. Met. Soc. Japan*, **75**, 181–189.

Ji, M., R. W. Reynolds and D. Behringer, 2000: Use of TOPEX/Poseidon sea level data for ocean analysis and ENSO prediction: Some early results. *J. Climate*, **13**, 216–231.

Johnson, G., B. M. Sloyan, W. S. Kessler and K. E. McTaggart, 2002: Direct measurements of upper ocean currents and water properties across the tropical Pacific during the 1990s. *Progress in Oceanography*, **52**, 31–61.

Kalnay, E., M. Kanamitsu, R. Kistler, W. Collins, D. Deaven, L. Gandin, M. Iredell, S. Saha, G. White, J. Whollen, Y. Zhu, M. Chelliah, W. Ebisuzabi, W. Higgins, J. Janowiak, K. C. Mo, C. Ropelewski, J. Wang, A. Leetmaa, R. Reynolds, R. Jenne and D. Joseph, 1996: The NCEP/NCAR 40-year reanalysis project. *Bull. Amer. Met. Soc.*, **77**, 437–471 .

Levitus, S., R. Burgett and T. P. Boyer, 1994: Salinity. World Ocean Atlas. *NOAA Atlas NESDIS 3, U.S. Deptartment of Commerce*, **3**, 99pp.

Lorenc, A. C., 2003: Modelling of error covariances by 4D-Var data assimilation. *Q. J. Roy. Meteor. Soc.*, **129**, 3167–3182.

Lukas, R. and E. Lindström, 1991: The mixed layer of the western equatorial Pacific ocean. *J. Geophys. Res.*, **96**, 3343–3457.

Madec, G., P. Delecluse, M. Imbard and C. Levy, 1998: OPA 8.1 Ocean General Circulation Model reference manual. *Notes du pôle de modélisation, Institut Pierre Simon Laplace (IPSL), France*, **11**, 91pp.

Maes, C. and D. Behringer, 2000: Using satellite-derived sea level and temperature profiles for determining the salinity variability: A new approach. *J. Geophys. Res.*, **105**, 8537–8548.

Maes, C., D. Behringer, R. W. Reynolds and M. Ji, 2000: Retrospective analysis of the salinity variability in the western tropical Pacific Ocean using an indirect minimization approach. *J. Atmos. Oceanic Technol.*, **17**, 512–524.

McPhaden, M. J., A. J. Busalacchi, R. Cheney, J. R. Donguy, K. S. Gage, D. Halpern, M. Ji, P. Julian, G. Meyers, G. T. Mitchum, P. P. Niiler, J. Picaut, R. W. Reynolds, N. Smith and K. Takeuchi, 1998: The Tropical Ocean-Global Atmosphere observing system: A decade of progress. *J. Geophys. Res.*, **103**, 14169–14240.

Picaut, J. and R. Tournier, 1991: Monitoring the 1979-1985 equatorial Pacific current transports with expendable bathythermograph data. *J. Geophys. Res.*, **96**, 3263–3277.

Reynolds, R. W. and T.M. Smith, 1994: Improved global sea surface temperature analyses using optimal interpolation. *J. Climate*, **7**, 929–948.

Roemmich, D., M. Morris, W. R. Young and J. R. Donguy, 1994: Fresh equatorial jets. *J. Phys. Oceanogr.*, **24**, 540–558.

Roemmich, D., O. Boebel, Y. Desaubies, H. Freeland, K. Kim, B. King, P.-Y. LeTraon, R. Molinari, W. Bechner Owens, S. Riser, U. Send, K. Takeuchi and S. Wijffels, 2001: Argo: The global array of profiling floats. In *Observing the oceans in the 21st century*. C. J. Koblinsky and N. R. Smith (Eds.), National Library of Australia Catalogue-in-Publication entry, pages 248–257.

Tarantola, A., 1987: *Inverse Problem Theory: Methods for Data Fitting and Model Parameter Estimation.* Elsevier, 613pp.

Troccoli, A. and K. Haines, 1999: Use of Temperature-Salinity relation in a data assimilation context. *J. Atmos. Oceanic Technol.*, **16**, 2011–2025.

Troccoli, A., M. Alonso Balmaseda, J. Segschneider, J. Vialard, D. L. T. Anderson, T. Stockdale, K. Haines and A. D. Fox, 2002: Salinity adjustments in the presence of temperature data assimilation. *Mon. Wea. Rev.*, **130**, 89–102.

Vialard, J. and P. Delecluse, 1998: An OGCM study for the TOGA decade. Part I: Role of the salinity in the Physics of the Western Pacific Fresh Pool. *J. Phys. Oceanogr.*, **28**, 1071–1088.

Vialard, J. and P. Delecluse, 1998: An OGCM study for the TOGA decade. Part II: Barrier layer formation and variability. *J. Phys. Oceanogr.*, **28**, 1089–1106.

Vialard, J., C. Menkes, J. -P. Boulanger, P. Delecluse, E. Guilyardi and M. J. McPhaden, 2001: A model study of the oceanic mechanisms affecting the equatorial SST during the 1997-98 El Niño. *J. Phys. Oceanogr.*, **31**, 1649–1675.

Vialard, J., P. Delecluse and C. Menkes, 2002: A modeling study of salinity variability and its effects in the tropical Pacific ocean during the 1993-99 period. *J. Geophys. Res.*, **107**, 8005, doi:10.1029/2000JC000758.

Vialard, J., A. T. Weaver, D. L. T. Anderson and P. Delecluse 2003: Three- and four-dimensional variational assimilation with a general circulation model of the tropical Pacific Ocean. Part 2: physical validation. *Mon. Wea. Rev.*, **131**, 1379–1395.

Vossepoel, F. C. and D. W. Behringer, 2000: Impact of sea level assimilation on salinity variability in the western equatorial Pacific. *J. Phys. Oceanogr.*, **30**, 1706–1721.

Weaver, A. T. and P. Courtier, 2001: Correlation modelling on the sphere using a generalized diffusion equation. *Q. J. Roy. Meteor. Soc.*, **127**, 1815–1846.

Weaver, A. T., J. Vialard and D. L. T. Anderson, 2003: Three- and four-dimensional variational assimilation with a general circulation model of the tropical Pacific Ocean. Part 1: formulation, internal diagnostics and consistency checks. *Mon. Wea. Rev.*, **131**, 1360–1378.
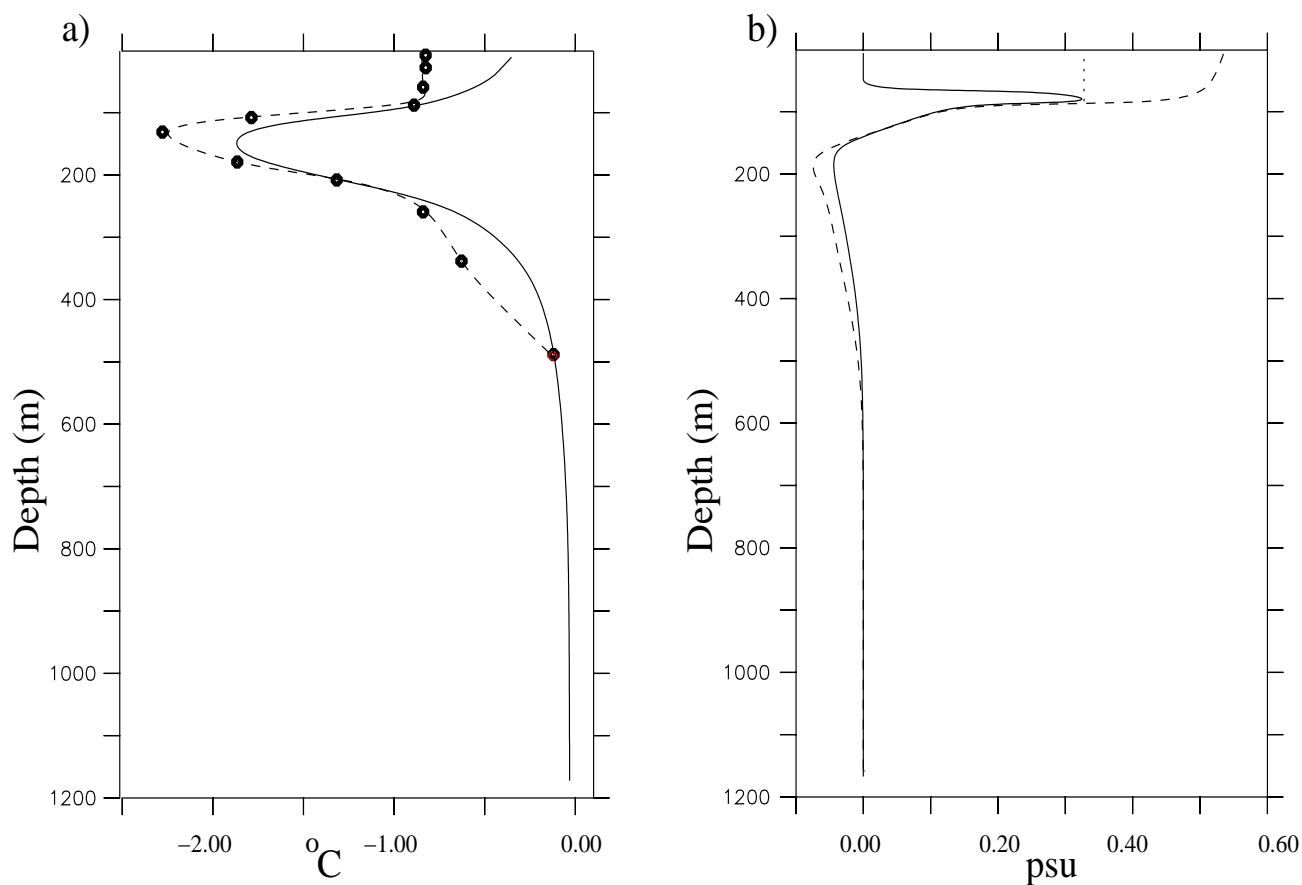
*Figure 1: A single profile twin experiment at 160°E on the equator. The "true" increment (dashed curve) and the 3D-Var analysis increment (solid curve) for a) temperature and b) salinity. The large dots in panel a correspond to the background-minus-observation differences (−**d** in Eq. 1) that were assimilated. The small dots in panel b represent the effect of extrapolating the balanced salinity increment at the base of the mixed layer directly to the surface.*
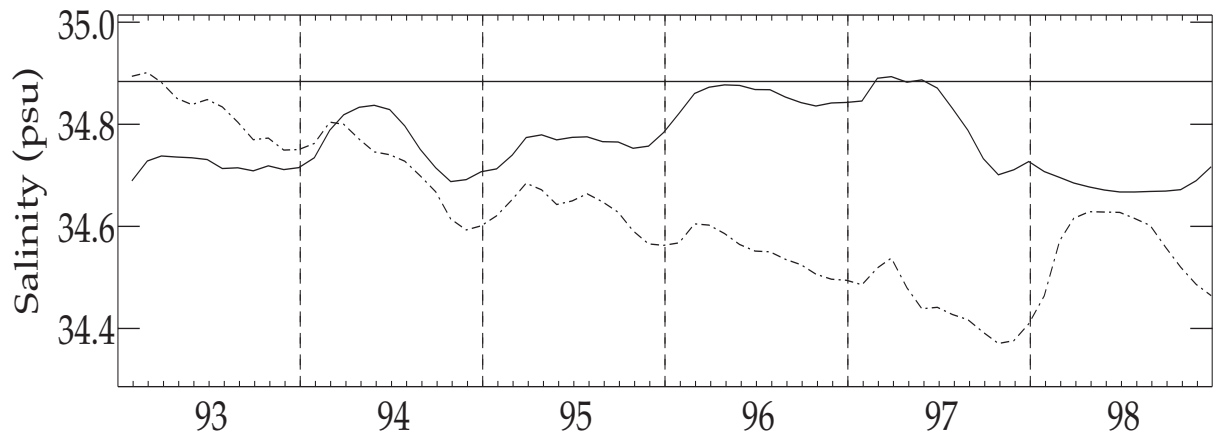
Figure 2: The averaged salinity for the univariate 3D-Var experiments performed with (NOTS) and without (EX3D) fresh water flux correction (solid and dashed-dotted curves, respectively) plotted as a function of time. The average is taken over the upper 50m of the ocean in the TAO region (defined as $160°E - 70°W; 10°S - 10°N$). The thick horizontal line indicates the Levitus climatological value.
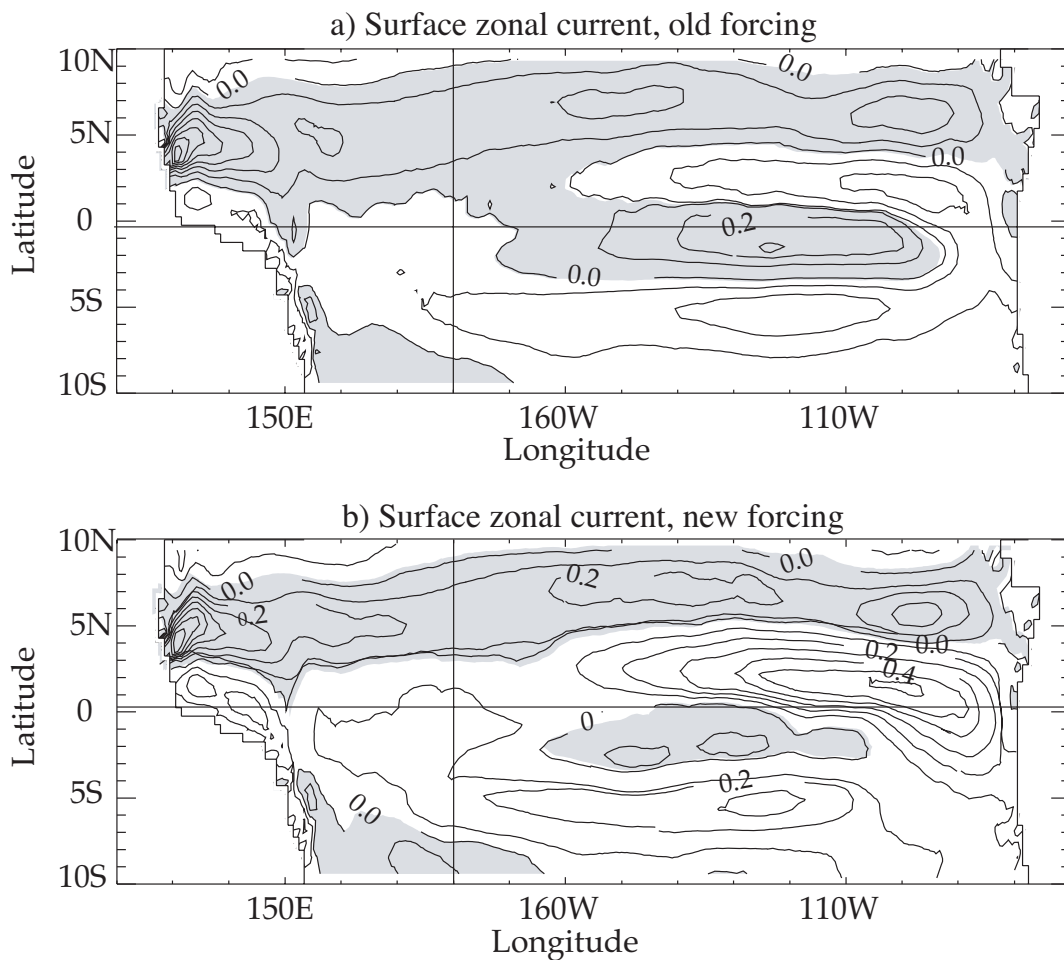
Figure 3: a) The 1993-98 zonal surface current climatology from a univariate 3D-Var experiment using a) ERS wind forcing (EX3D) and b) ERS-TAO wind forcing (NOTS). The contour interval is $0.1 m.s^{-1}$.

a) Levitus

b) 3D-Var with T-S constraint

c) 3D-Var without T-S constraint

d) Control
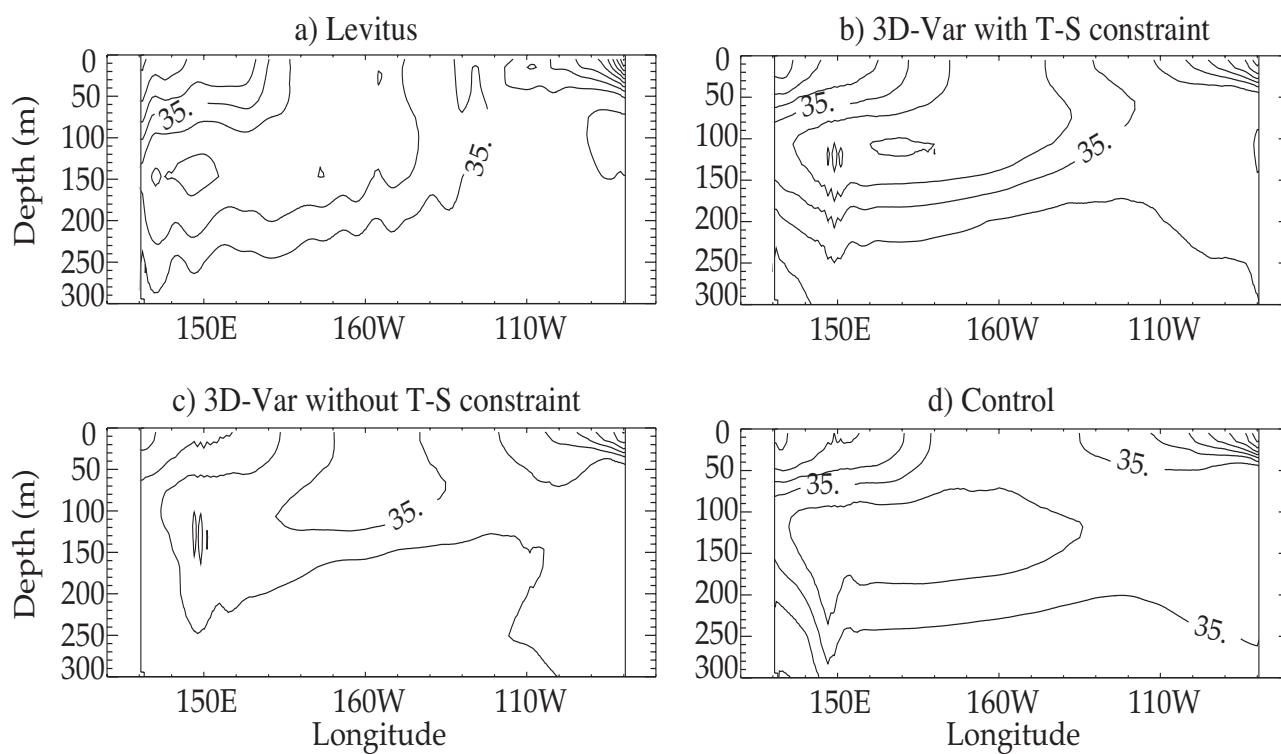
Figure 4: Depth section along the equator of the 1993-98 salinity climatology from a) Levitus, b) TS, c) NOTS and d) CTL. The contour interval is 0.2psu.
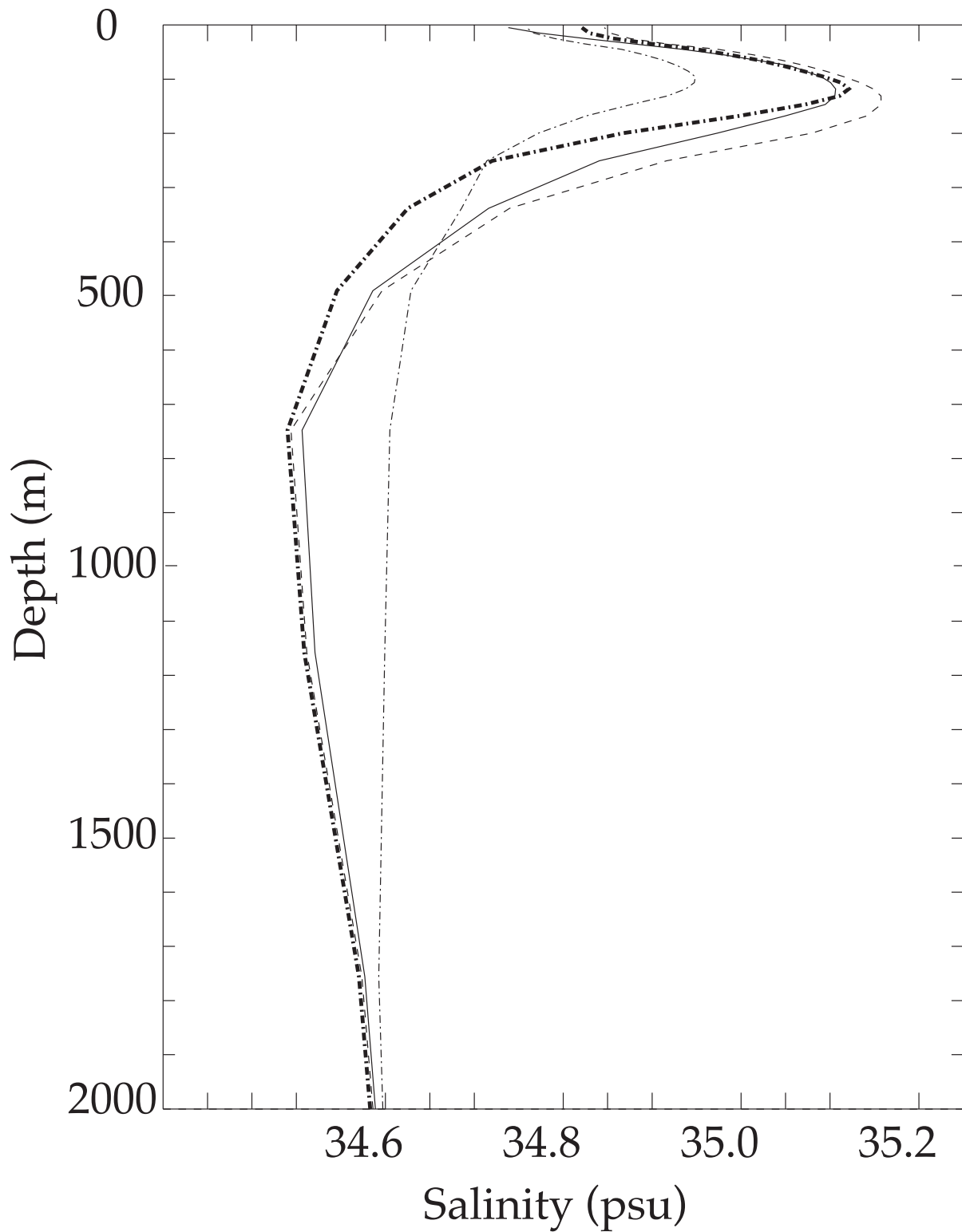
Figure 5: The 1996 mean salinity profile between 0-2000m averaged over the TAO region: Levitus climatology (solid curve), CTL (dashed curve), NOTS (thin dashed-dotted curve) and TS (thick dashed-dotted curve).
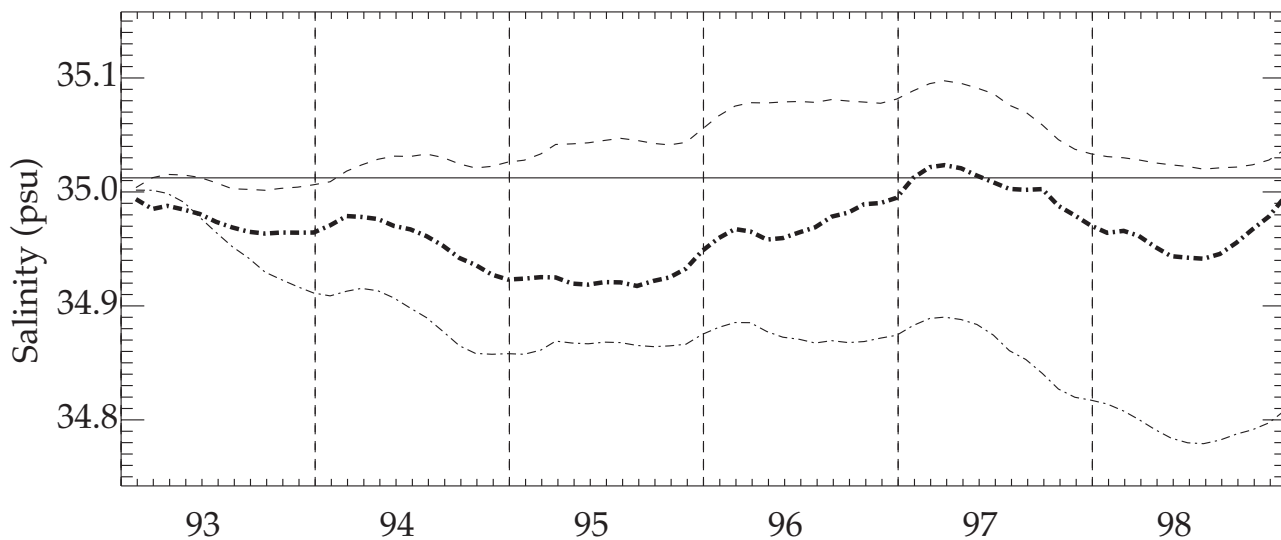
Figure 6: *The averaged salinity over the upper 300m of the TAO region for CTL (dashed curve), NOTS (thin dashed-dotted curve) and TS (thick dashed-dotted curve) plotted as a function of time. The thick horizontal line indicates the Levitus climatological value.*
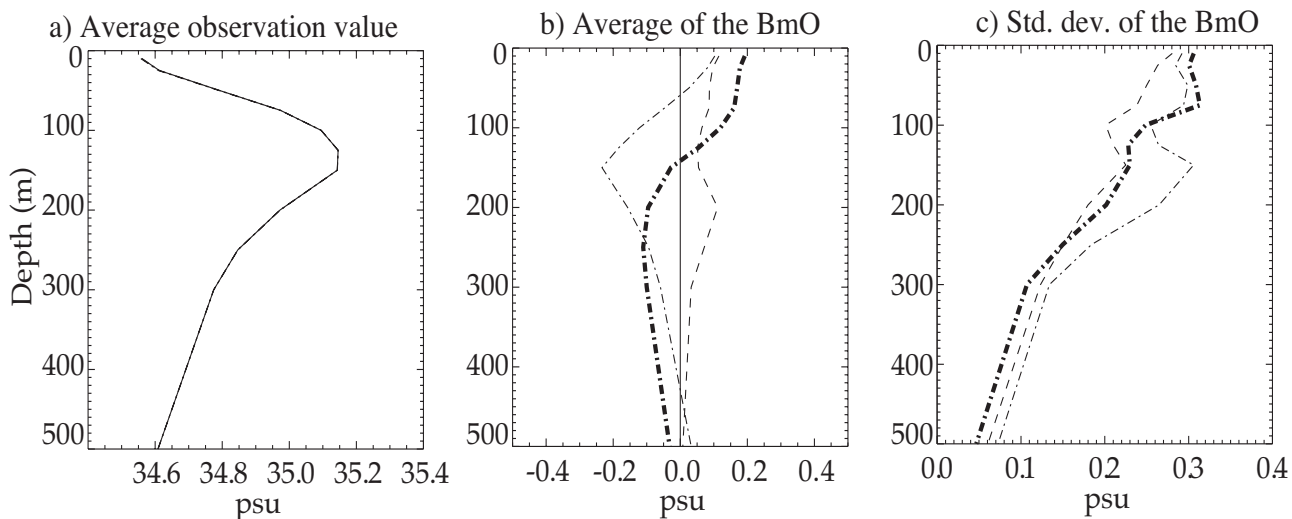
Figure 7: *Statistics of the BmO, time averaged over the 1993-98 period and spatially averaged over the TAO region, plotted as a function of depth. a) The average observation value from the Johnson* et al. *(2002) data-set; b) the average of the* BmO*; and c) the standard deviation of the* BmO*. In panels b and c), dashed curves correspond to CTL, thin dashed-dotted curves to NOTS and thick dashed-dotted curves to TS.*

a) Average of the BmO

b) Std. dev. of the BmO
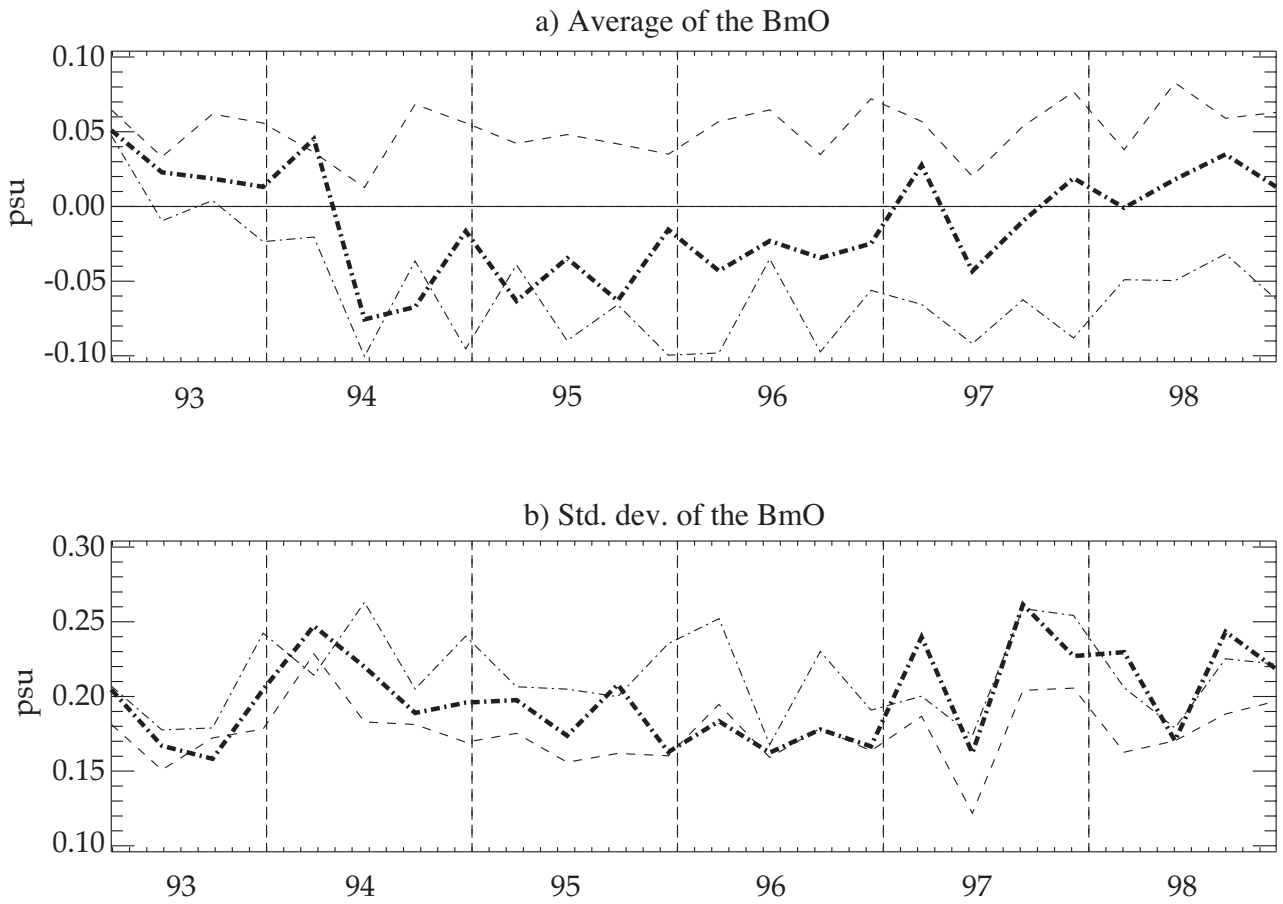
Figure 8: Statistics of the BmO, spatially averaged over the upper 300m of the TAO region, plotted as a function of time. a) The average of the BmO; and b) the standard deviation of the BmO. Dashed curves correspond to CTL, thin dashed-dotted curves to NOTS, and thick dashed-dotted curves to TS.

3D-Var with T-S constraint
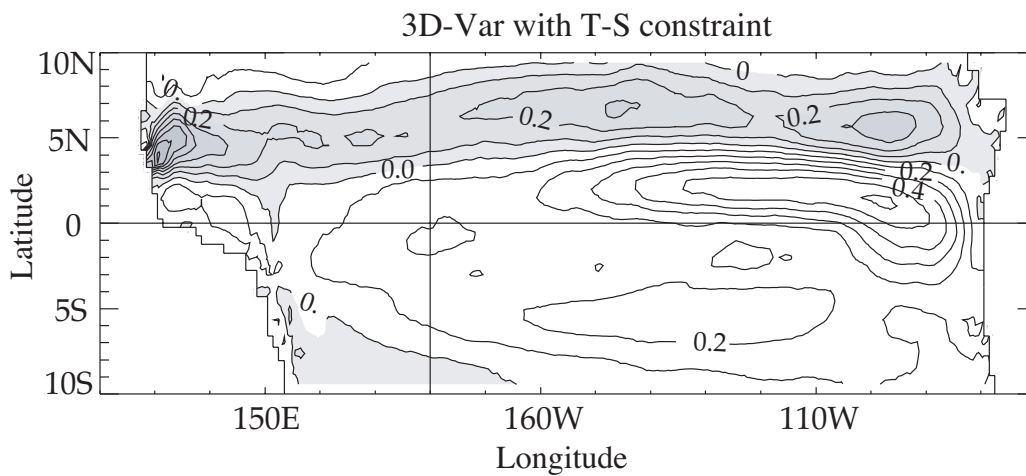
Figure 9: The 1993-98 zonal surface current climatology for TS. The contour interval is $0.1 \mathrm{m \cdot s}^{-1}$.

a) Currents at 165°E

b) Currents at 140°W

c) Currents at 110°W
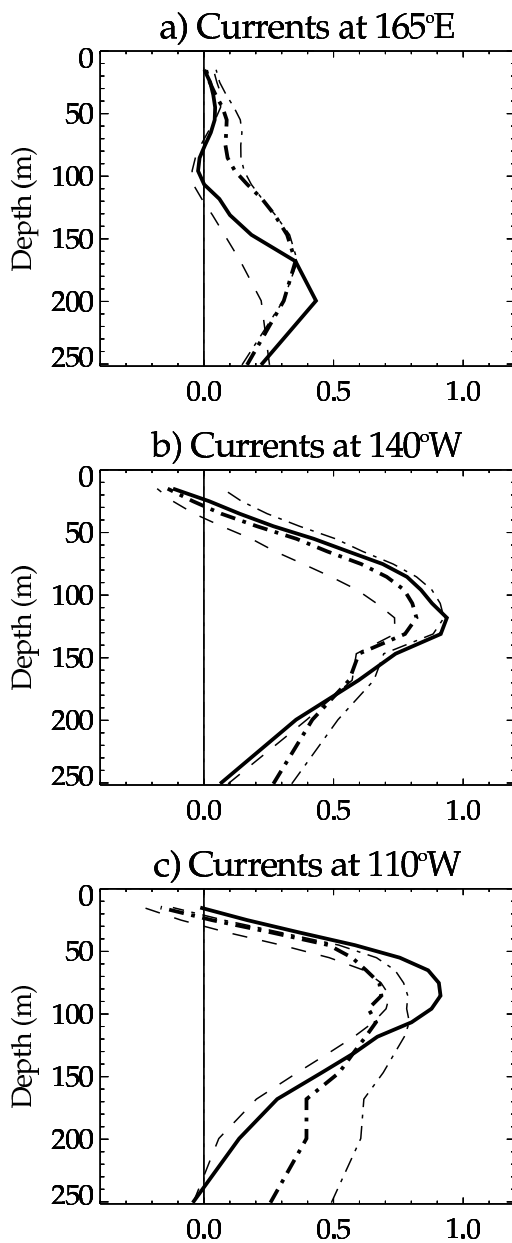
Figure 10: Vertical profiles of the 1993-98 averaged zonal currents at the equator from TAO (thick solid curve), CTL (dashed curve), NOTS (thin dashed-dotted curve) and TS (thick dashed-dotted curve). The model values have been sampled in the same way as the data (i.e., when there are gaps in the data, no model values are used).

a) Control

b) 3D-Var without T-S constraint

c) 3D-Var with T-S constraint
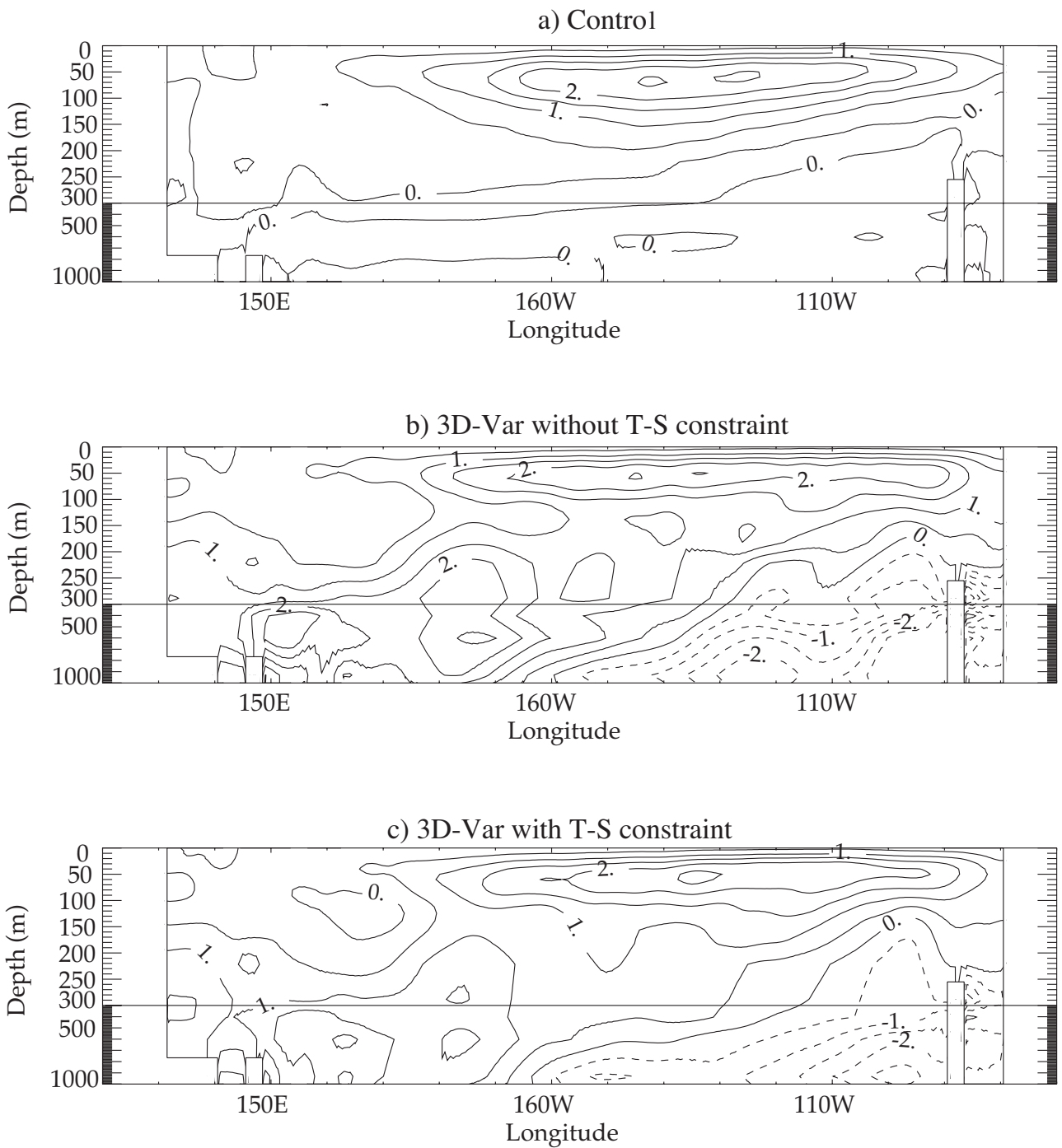
Figure 11: Depth section along the equator of the 1993-98 averaged vertical velocities from a) CTL, b) NOTS and c) TS. The contour interval is $0.05\mathrm{m.day}^{-1}$. Dashed contours indicate downwelling.

a) ΔT (°C)

b) ΔS (psu)

c) ΔHdyn (cm)

d) Δu (m/s)
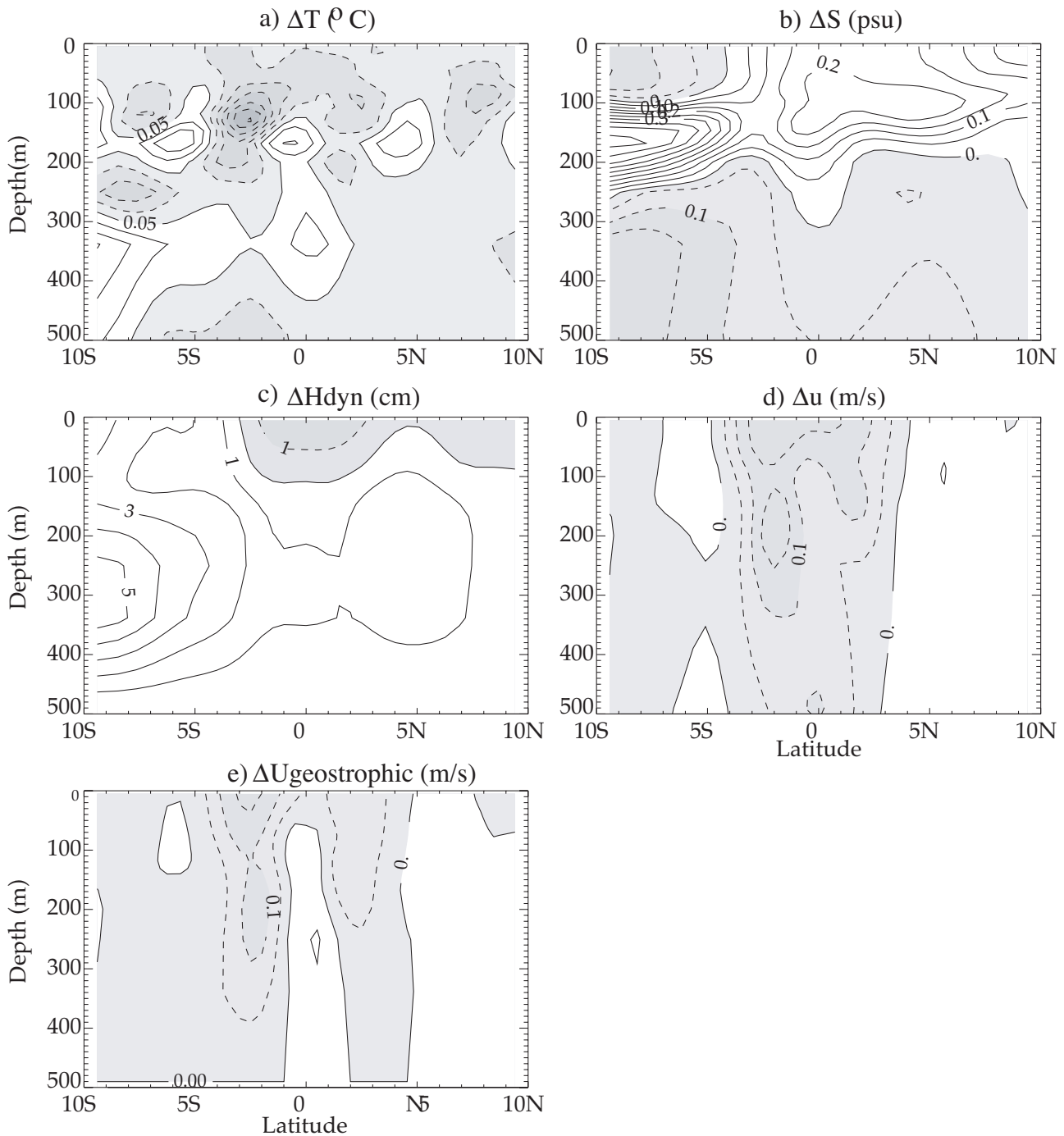
e) ΔUgeostrophic (m/s)

Figure 12: Depth section of the 170°W–120°W zonally averaged difference between 1993-98 averaged fields from TS and NOTS: a) temperature; b) salinity; c) dynamic height referenced to 1500m; d) zonal velocity; and e) the geostrophic component of the zonal velocity computed from the dynamic height difference in panel c. The contour interval is 0.1 °C in panel a, 0.05 psu in panel b, 1cm in panel c, and 0.05m.s⁻¹ in panels d and e.
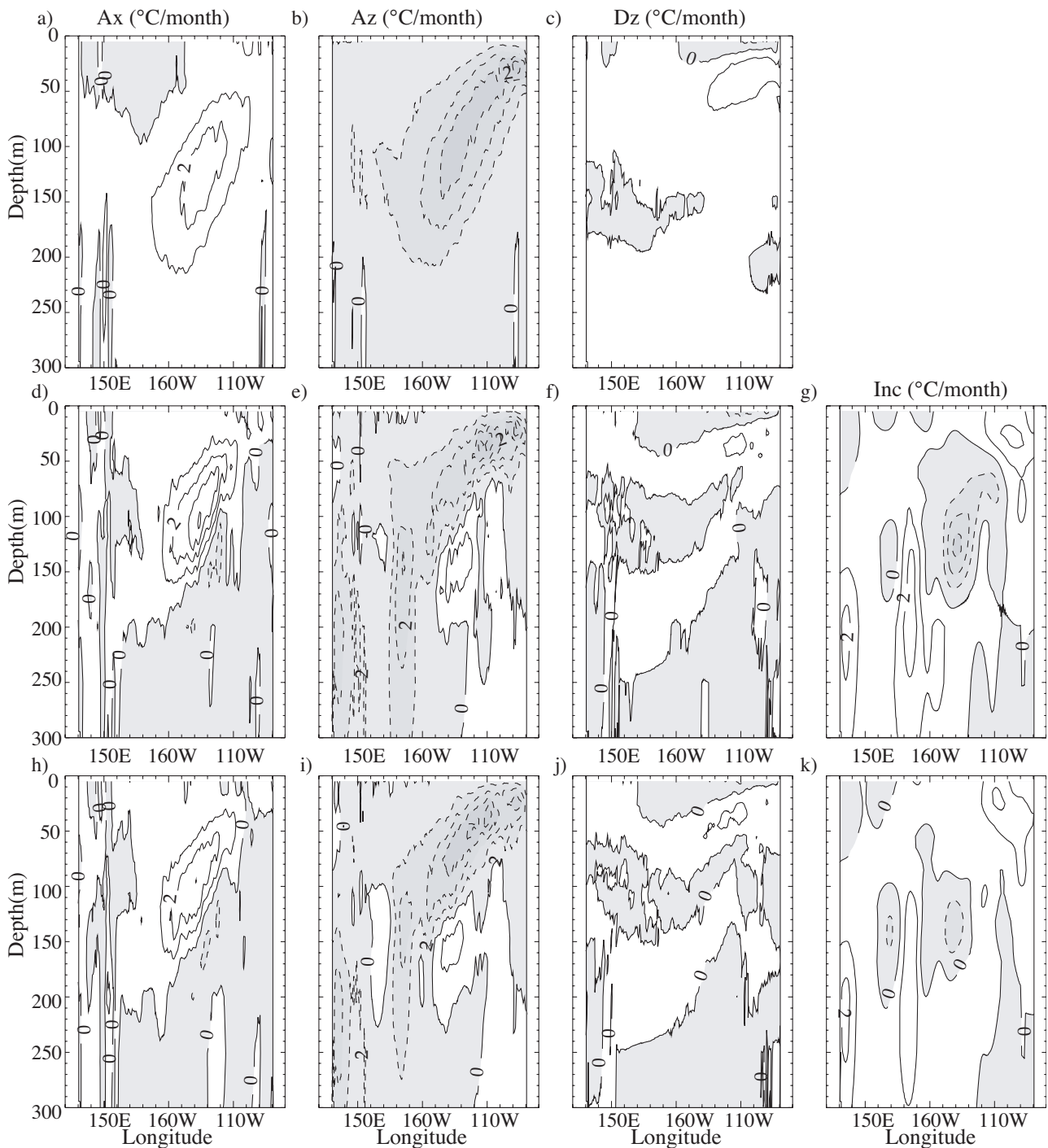
Figure 13: Heat budget. Depth section averaged between 1°S–1°N of the 1993-98 mean contributions per month from zonal advection (a, d, h), vertical advection (b, e, i), vertical diffusion (c, f, j) and the temperature analysis increment (g, f) for CTL (a, b, c), NOTS (d, e, f, g) and TS (h, i, j ,k). The contour interval is 1°C.
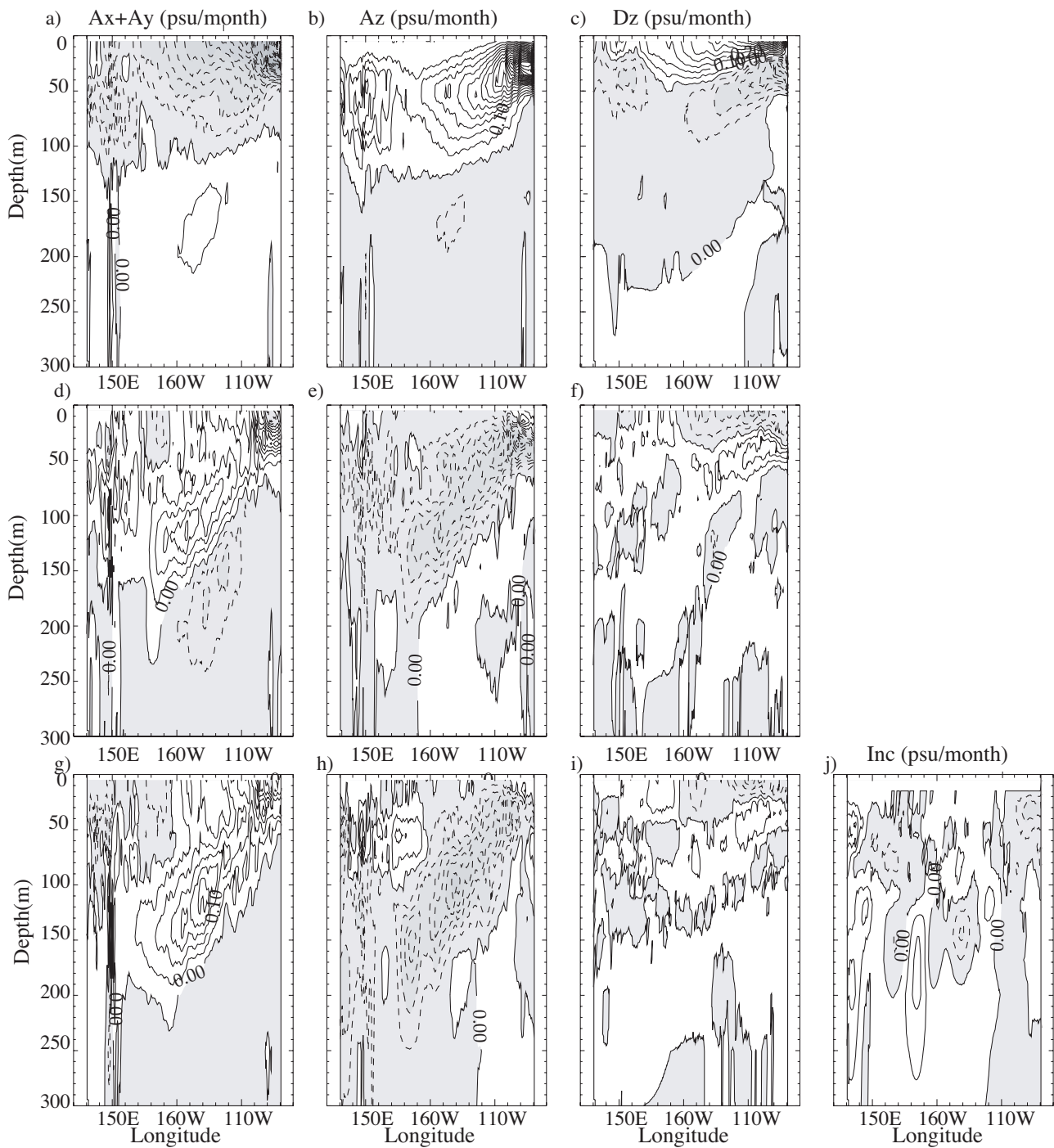
Figure 14: Fresh water budget. Depth section averaged between $1°S$–$1°N$ of the 1993-98 mean contributions per month from horizontal (zonal + meridional) advection (a, d, g), vertical advection (b, e, h), vertical diffusion (c, f, i) and the salinity analysis increment (j) for CTL (a, b, c), NOTS (d, e, f) and TS (g, h, i, j). The contour interval is 0.05 psu.
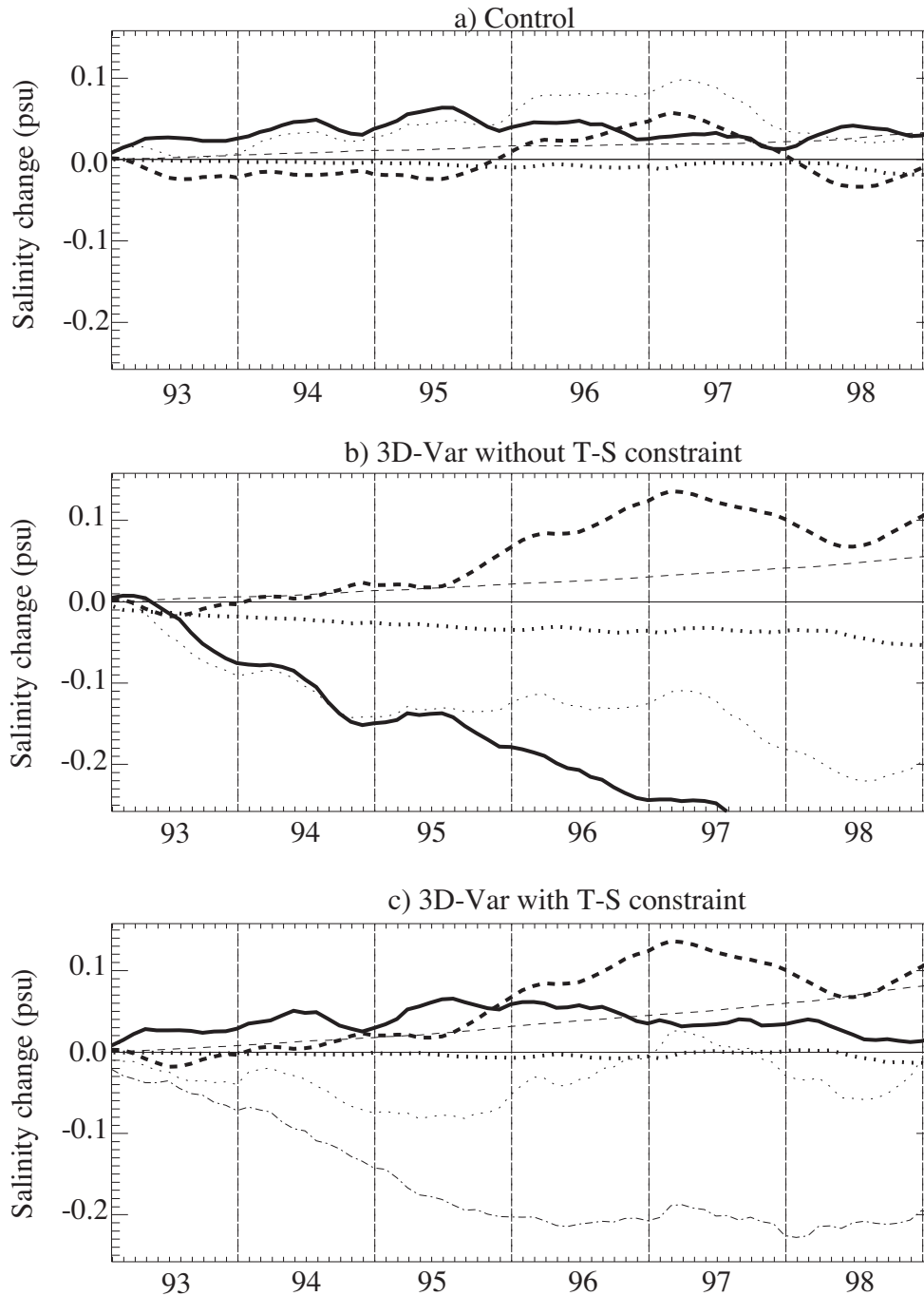
Figure 15: Fresh water budget. Time accumulated contributions, averaged over the upper 300m of the TAO region, from horizontal and vertical advection (thick solid curve), horizontal diffusion (thin dashed curve), surface forcing (thick dashed curve) and vertical diffusion (thick dotted curve) for a) CTL, b) NOTS and c) TS. The dashed-dotted curve in panel c corresponds to the salinity increment, the thin dotted curves in panels a, b, and c correspond to the sum of the contributions as presented in Fig. 6.